Biochemical Studies of Cardiac Calsequestrin; Its Interaction with Pharmaceutical Drugs and Its Deleterious Mutations

By

EUNJUNG KIM

A dissertation submitted in partial fulfillment of

the requirements for the degree of

DOCTOR OF PHILOSOPHY

WASHINGTON STATE UNIVERSITY

School of Molecular Biosciences

May 2007

To the Faculty of Washington State University:

The members of the Committee appointed to examine the dissertation of EUNJUNG KIM find it satisfactory and recommend that it be accepted.

_____

Chair

_____

_____

_____

ACKNOWLEDGEMENT

I expressed my sincere thanks to all who have helped me throughout the graduate study:

Specifically, I would like to express my heart-felt gratitude to my advisor, Dr. ChulHee Kang, without his support, precious advice with insight, enthusiasm and guidance, this work would not have been possible. I am honored to have been trained by him to be a better scientist and wish him good luck in all his endeavors. I also want to thank my thesis committee members, Dr.Thomas W.Okita, Dr. Bill Davis, and Dr.James Bruce for their assistance and the constructive suggestions throughout these years.

Next, I would like to thank all the past and present members of Dr.Kang lab who have helped me in countless ways over the years; Dr. HaJeung Park, Dr. IlYoung Park, Ms. HyeKyoung Kim and Mr. Lenord Kemper for their visible or invisible help. Specifically, I would like to thank Dr. BuHyun Youn who has affected my graduate life and study in choosing Dr.Kang's lab and getting a Ph.D.

Finally, I want to thank my husband, HongSoo Choi for his dedication and unlimited support. Here again, without his support my graduate study would not have been possible. I also express my thanks to my parents JunKi Kim, TaeSun Shin, my mother in law, JumSun Kim, my sister EunKyoung Kim, my brothers JinYup Kim and JinHoon Kim for their support and encouragement from Korea and my daughter Sophia EunYoung Choi for her entertainment throughout these days.

Biochemical Studies of Cardiac Calsequestrin; Its Interaction with Pharmaceutical Drugs and Its Deleterious Mutations

Abstract

By EunJung Kim, PhD

Washington State University

May 2007

Chair: ChulHee Kang

Calsequestrin is a high capacity but low affinity Ca^{2+} binding protein located in the lumen of Sarcoplasmic Reticulum (SR) whose primary function is to maintain Ca^{2+} concentration at the level of 10^{-3} ~10^{-4} M. Calsequestrin is an essential key protein in the process of muscle contraction by controlling the SR Ca^{2+} release and by serving as a Ca^{2+} sensor for the ryanodine receptor, which is a Ca^{2+} release channel.

In this dissertation, the first two chapters are concentrated on the description of drugs and mutational effects on the Ca^{2+} regulatory function of calsequestrin. The last chapter, I report a preliminary structural study of canine cardiac junctin, one of the calsequestrin anchoring proteins, required for mediating the normal operation of Ca^{2+} regulatory function of calsequestrin.

TABLE OF CONTENTS

Dedication

This dissertation is dedicated to my parents and my husband.

CHAPTER ONE

EFFECTS OF DRUGS WITH MUSCLE-RELATED SIDE EFFECTS AND AFFINITY FOR CALSEQUESTRIN ON THE CALCIUM REGULATORY FUNCTION OF SARCOPLASMIC RETICULUM MICROSOMES

Preface

Calsequestrin is a Ca^{2+} storage protein located in the lumen of the Sarcoplasmic Reticulum (SR). Calsequestrin actively participates in the process of muscle contraction by controlling the luminal Ca^{2+} concentration in both cardiac and skeletal muscle.

According to the crystal structures of cardiac and skeletal calsequestrins, calsequestrins are composed of thioredoxin-like folds containing a five β stranded sheet sandwiched by four α helices. Almost without exception, these thioredoxin folds either form a crevice which binds small ligands or has a redox site at a specific locus. These sites in calsequestrin are predicted to be binding sites for the small ligands.

We previously observed that some types of drugs with heart related side effects such as tachycardia, bradycardia, palpitation and sudden cardiac death bind calsequestrin with Kd in the micromolar range. The consequences of their interaction included a significant reduction in the Ca^{2+} binding capacity of calsequestrin. Therefore, it was proposed that better understanding of the molecular mechanism of calsequestrin-drug interactions could lead to modification of drug molecules with reduced heart related side effects.

In the following manuscript, we examined the effects of these drug-calsequestrin interactions on the SR microsomes to further understand the molecular details of undesirable drug effects. this manuscript was published by *Molecular Pharmacology in September*, 2005.

Effects of Drugs with Muscle-Related Side Effects and Affinity for Calsequestrin on the Calcium Regulatory Function of Sarcoplasmic Reticulum Microsomes

EunJung Kim, Maggie Tam, William F. Siems, and ChulHee Kang

Department of Chemistry (M.T., W.F.S., C.K.) and School of Molecular Biosciences (E.K., C.K.), Washington State University, Pullman, WA 99164-466

Running title: Adverse interaction between cardiac calsequestrin and a certain type of drugs.

Summary

The tight regulation of Ca^{2+} release to and clearance from the cytosol is essential for normal excitation-contraction coupling in both skeletal and cardiac muscles. Calsequestrin (CSQ) is one of the major components in the sarcoplasmic reticulum (SR) of both skeletal and cardiac muscle. Previously, we showed that several pharmaceutical drugs, such as phenothiazine derivatives, tricyclic antidepressants, anthracycline derivatives, and other hydrophobic compounds bind CSQ with K_d values in the micromolar range and significantly reduce the Ca^{2+} binding capacity of cardiac CSQ (1). Because of its key role in Ca^{2+} regulation, this interference with CSQ function could well produce adverse physiological consequences and potentially be linked to the known muscle-related side effects of these drugs. To further understand the molecular mechanism of undesirable drug effects or adverse drug reactions among those compounds, we examined their effect on the SR microsome. The results clearly showed that these compounds affect Ca^{2+} release and reduce the total Ca^{2+} content of the purified SR microsomes, matching well with our previous results with purified recombinant CSQ. Liquid chromatography-mass spectrometry/mass spectrometry showed that the antipsychotic drug trifluoperazine penetrates well into the SR microsome as expected from the reported and calculated log *S* (aqueous solubility) and log *P* (partition coefficient) values among the phenothiazine derivatives. We therefore propose that a certain portion of the muscle-related (both cardiac and skeletal) complications of these drugs is caused by the altered Ca^{2+} regulation of the SR mediated by their adverse interaction with CSQ.

FOOTNOTES AND ABBREVIATIONS

This work was supported by National Science Foundation (MCB-0117192), the American Heart Association, and the Murdock Charitable Trust.

The abbreviations used are:

SR, sarcoplasmic reticulum

TFP, trifluoperazine

CSQ, calsequestrin

DMSO, dimethyl sulfoxide

RyR, ryanodine receptor

MOPS, 4-morpholinepropanesulfonic acid

LC-MS/MS, liquid chromatography-mass spectrometry/mass spectrometry

c, cardiac

s, skeletal.

Introduction

The sarcoplasmic reticulum (SR) plays an essential role in muscle excitation-contraction coupling by regulating the cytosolic free Ca^{2+} concentration. The main SR proteins responsible for this Ca^{2+} regulation are the Ca^{2+} transport ATPase, the Ca^{2+} release channel ryanodine receptor, and the Ca^{2+} storage protein calsequestrin (CSQ). Among these, CSQ represents a ubiquitous, critically important Ca^{2+} storage protein found not only in the SR but also in the endoplasmic reticulum. CSQ binds 60 to 80 Ca^{2+} ions per molecule with a binding constant of approximately 1 mM under physiological conditions (2; 3) CSQ acts as a Ca^{2+} buffer inside the SR, lowering free Ca^{2+} concentrations in SR and thereby facilitating further uptake by the Ca^{2+}-ATPases. It also actively participates in muscle contraction by localizing Ca^{2+} at the release site and regulating the size of the functional Ca^{2+} store in SR through an interaction with the ryanodine receptor (RyR) (4; 5; 6).

We determined the structures of rabbit skeletal CSQ (7)and canine cardiac CSQ (8). Both cardiac CSQ (cCSQ) and skeletal CSQ (sCSQ) contain three similar thioredoxin-like domains, a basic motif that often provides the platform for small-molecule binding (3; 7; 9; 10). Individual thioredoxin-like domain, which is composed of ~100 residues, has a five-stranded β-sheet sand-wiched between four α-helices. These potential binding sites occur at chain reversals that generate a crevice defined by the edge of one βsheet and the carboxyl ends of the adjacent β2 and β3 strands (9). Not only are these sites in both CSQs predicted to be binding sites from the topology diagrams, these sites also form hydrophobic grooves that

are bound by exposed hydrophilic side chains, with considerable structural similarity to binding sites in other open-sheet structures.

One of the phenothiazine-derived antipsychotic drugs, trifluoperazine (TFP), was reported to change the conformation and Ca^{2+} binding properties of sCSQ (12) and to impair the normal excitation-contraction coupling of muscle (13), reflecting its known adverse effect on normal Ca^{2+} regulation of both cardiac and skeletal muscles. In addition to their typical muscle-related side effects such as uncontrollable muscle movements (trembling and shaking), severe muscle stiffness, and spasms, TFP and other phenothiazine-based antipsychotic drugs often induce QTc prolongation (14), polymorphic ventricular arrhythmia (15; 16) and sudden death (14; 17; 18). For these reasons, intentional use of this type of drug even for suicidal purposes has become common) (19).

Therefore, to further confirm the existence of a small-molecule binding site in CSQ and to investigate the consequence of binding, we carried out studies with TFP and other pharmaceuticals, such as phenothiazine derivatives, tricyclic antidepressants, and anthracycline derivatives that have reported muscle-related side effects (such as tachycardia, bradycardia, palpitation, changing P-R, QRS, QTc prolongation, heart failure, etc.) for their binding affinity to CSQ using isothermal calorimetry (1). The results showed that most of the drugs which belong to phenothiazine, anthracycline, and tricyclic derivatives bind cCSQ with K_d values in the micromolar range. In most cases, binding is enthalpically driven and slightly entropically unfavorable, possibly indicating that the structure is slightly stabilized upon ligand binding. Fluorescence quenching studies also demonstrated that TFP, daunorubicin, and daunorubicinol bind to CSQ with apparent binding affinities in the micromolar rang (13).

The similar binding patterns were observed for the rabbit sCSQ (E. Kim and C. Kang, unpublished data).

Upon binding, those compounds with a low K_d significantly reduced the Ca^{2+} binding capacity of cCSQ. Furthermore, fluorescence spectroscopic data for 8-anilino-1-naphthalene sulfonate binding to cCSQ closely resembles 8-anilino-1-naphthalene sulfonate binding to flavine or nucleotide-binding sites (1). On the other hand, common small molecules, which have flat multiring structures, such as $NADP^+$, FAD, ATP, GTP, caffeine, adenine, guanine, tetracycline, riboflavine, and quinine, did not show any significant binding. In addition, TFP and promethazine bind cCSQ, but similarly structured thioridazine does not, indicating a potential regiospecificity in that interaction (1).

When this information is combined with the high membrane permeability of these hydrophobic multiring drugs, our results lead us to the hypothesis that there could be undesirable and damaging interactions between CSQ and these pharmaceutical compounds, generating various muscle-related side effects. The very high local concentration (100 mg/ml) of CSQ within the lumen of the SR guarantees that even low blood concentrations of these drugs (approximately micromolar range for K_d values) can be sufficient to lead to binding and thereby to serious physiological consequences. A slight alteration in the normal physiological function of the cardiac SR may be enough to cause problems in many individuals. In addition, long-term treatment with such drugs could easily generate a cumulative effect, producing a non-negligible problem (long-term toxicity). Cardiotoxicity especially has been known to be a serious side effect of many pharmaceutical drugs whose

clinical usefulness is often limited by both dose- and time-dependent body accumulation and subsequent toxicity.

Just like the phenothiazine-derived antipsychotic drugs, the anthracycline-derived anti-cancer drugs, such as widely used and highly effective doxorubicin and daunorubicin, produce severe cardiotoxicity, often irreversibly damaging the heart, which somewhat limits their therapeutic potential (20; 21). The pathophysiological and biochemical reasons for these side effects are not well understood. If our hypothesis is corrt, then the discovery of alternative molecules with reduced affinity for CSQ provides a strategy for developing drug molecules with reduced skeletal and cardiac-related adverse drug reaction.

Previously, we reported that binding by certain kinds of drugs significantly reduces the total amount of Ca^{2+} bound to CSQ (1). However, uncertainty still exists as to whether the observation that a certain class of small, hydrophobic ligands interferes with Ca^{2+} binding by purified recombinant cCSQ is relevant to CSQ function in vivo. The experiments ignored the importance of the membrane barrier and post-translational modification of cCSQ, such as phosphorylation and glycosylation (22). Recently, severe inhibition of the caffeine-induced Ca^{2+} release rate from SR microsome by TFP and several other drugs, such as anthracycline derivatives, was reported (13). Therefore, to characterize this potential interdependency between drug binding and Ca^{2+} regulation more thoroughly, we performed the experiments with the set of drugs that have a significant affinity for CSQ using purified SR microsomes.

Materials and Methods

Preparation of SR Vesicles: SR microsomes were isolated from the white skeletal muscle of rabbits by the method described previously (12; 23; 7). After removing fat and connective tissues, both back and leg muscles were ground in a meat grinder and approximately 50 g of ground meat in 250 ml of 0.3 M sucrose and 5 mM imidazole-HCl, pH 7.4, were homogenized three times for 30 s each at the maximal speed using a Waring blender (Waring Laboratory, Torrington, CT). The homogenate was centrifuged for 10 min at 7700*g*, followed by filtration of the supernatant through six to eight layers of cheesecloth. Microsomal pellets were obtained by centrifuging the supernatant for 30 min at 110,000*g*. Pellets were resuspended in 0.3 M sucrose and 5 mM imidazole-HCl, pH 7.4, and were stored at -70°C. Protein concentration was determined by the Lowry method.

SR Calcium Loading: SR microsomes were incubated for 1 h in a buffer solution (20 mM MOPS, pH 7.5, 50 mM KH_2PO_4, 5 mM KCl, 2 mM $MgCl_2$, and 2 mM ATP) with various target drugs and without drug as a control. Most of the drugs were dissolved in deionized water. Two water-insoluble compounds, L-tryptophan and tetracycline were dissolved in DMSO. After incubation, 7 nmol of $CaCl_2$ was added to the buffer containing SR microsomes to fully load Ca^{2+} into the microsome by following the method described previously (24). Quite often, more than 10 times of this loading process triggered Ca^{2+}-induced Ca^{2+} release from SR microsomes; thus, the loading was repeated up to 10 times (24). Data were obtained through the difference absorbance spectrum (A_{710}–A_{790}) of free Ca^{2+} in solution using the metallochromic indicator antipyrylazo III and a diode array spectrophotometer (HP 8452A; Hewlett Packard, Palo Alto, CA).

Mass Spectroscopy: The amount of TFP inside of the incubated microsome was checked by modifying a method established previously (25). Each aliquot was acidified with 10 mM HCl for 5 min and then alkanized with 30% NH_4OH and vortexed for 5 min, followed by the additional of 1.5% isoamyl alcohol in heptane. The sample was then centrifuged at 1000*g*, and the heptane layer was collected repeatedly. The combined heptane extracts were evaporated to dryness with a SpeedVac (Thermo Electron, Waltham, MA) and reconstituted with 30 µl of liquid chromatography mobile phase (35% 20 mM ammonium acetate, 0.035% acetic acid, and 65% of acetonitrile). LC-MS/MS was performed on an Agilent-1100 series LC system (Agilent Technologies, Palo Alto, CA) with Microbore C_{18} column (Micro-Tech Scientific Inc., Vista, CA) coupled to an API 4000 triple quadruple mass spectrometer with electrospray ionization source (Applied Biosystems, Foster City, CA). The mass spectrometer was operating in selective reaction monitoring mode, observing parent ion of 408.1 Da and product ion of 113.2 Da (Fig. 2). The sample and calibration standards were run in triplicate.

Atomic Absorption Spectrophotometry: The total amount of calcium in the SR microsomes was analyzed using an Atomic Absorption Spectrophotometer (Shimadzu, Kyoto, Japan) at the absorption wavelength of 422.7 nm. After ultracentrifugation, the SR microsome pellet was dissolved in HCl overnight and then vaporized in a flame. Calcium concentration was determined after calibrating the instrument with a series of standard solutions of $CaCl_2$ (Fluka Chemical Corp., Ronkonkoma, NY). Protein content for individual pellets was assayed by the Lowry method to normalize calcium content.

Calcium Release Effect of TFP: The Ca^{2+} was loaded to SR microsomes following the 10-step process, as described above. To investigate the effect of TFP, the final Ca^{2+} loading step was immediately followed by adding TFP to a final concentration of 0.2 mM,

and the Ca^{2+} release was measured by monitoring the absorbance changes of 710 and 790 nm through the diode array spectrophotometer (HP 8452A). To check whether the observed TFP-induced Ca^{2+} release can be blocked by an RyR channel blocker, ruthenium red was added to the solution containing Ca^{2+}-loaded SR microsomes to a final concentration of 10 or 20 μM at 20 s after the application of TFP.

Results

To determine whether a given ligand that has a significant binding affinity to CSQ and reduces the Ca^{2+}-binding capacity of CSQ affects the total Ca^{2+} amount of SR microsomes, we performed ATP-dependent Ca^{2+} loading into purified rabbit skeletal SR microsomes. Each 7 nmol Ca^{2+} addition to the buffer that contains SR microsomes shows similar absorbance changes up to ~10 times loading (Fig. 1A). As shown in Fig. 1B of the Atomic Absorption Spectrophotometer data, the total amount of calcium in the SR microsomes was gradually increased reaching a plateau. This indicates that Ca-ATPase functioned properly to uptake Ca^{2+} into the lumen of SR microsome, and abnormal Ca^{2+} leakage out of SR microsome did not occur during the Ca^{2+} loading experiment. Sets of parallel SR calcium-loading experiments were performed with and without drugs that have the potential to cause short- and/or long-term cardiotoxicity, such as the following: 1) phenothiazine derivatives, including TFP, promethazine, and chlorpromazine; 2) tricyclic antidepressants, including nortriptyline, amitrityline, and imipramine; and 3) two anthracycline-based anticancer drugs, daunorubicin and doxorubicin. All of these compounds have micromolar range affinity to cCSQ and an inhibitory effect on its calcium binding capacity (1). The potential (skeletal and cardiac) muscle-related side effects of these drugs range from involuntary movements of muscles (dyskinesias) to arrhythmias and sudden death from heart failure.

Effect of Diffused Drugs on Ca^{2+} Storage Capacity of the SR Microsome: To study the effect of the cCSQ-binding drugs on the Ca^{2+} storage capacity of SR microsomes, microsomes were preincubated for 1 h with 1 mM concentration of either cCSQ binding or control drugs.

First, to quantify the amount of drugs that diffused into the SR microsomes, LC-MS/MS was performed for one of the target drugs, TFP (Fig. 2). The data show that the treated SR microsomes holds 1.02 ± 0.02 μg of TFP per 1 mg of SR microsomes that was incubated for 1 h in a buffer containing 1 mM TFP (Table 1). Even after rinsing the microsome pellet with fresh buffer twice, the SR microsome still contains 0.75 μg of TFP per 1 mg of SR microsomal pellet (Table 1).

After the 1-h incubation with and without drugs, 10 times Ca^{2+} loading was done as described under *Materials and Methods*. After this Ca^{2+} loading, each tube was immediately ultracentrifuged, and the SR pellet was incubated in HCl until it completely dissolved. The total amount of calcium in each tube was analyzed by atomic absorption spectroscopy; Table 2 and Fig. 3 show the normalized values. The total Ca^{2+} content of the tube, of which SR microsomes was loaded with Ca^{2+} (10 times) in the absence of any drug, was considered to be 100% for each set of experiments. As shown in Table 2 and Fig. 3, in every case, the SR microsome that was exposed to the CSQ binding drugs showed a significantly lower level of total calcium content compared with that of Ca^{2+}-loaded SR microsomes without drug preincubation. Among the tested drugs, TFP is the strongest inhibitor (~40% inhibition at 1 mM concentration) of calcium storage capacity, which is somewhat in agreement with our previous results by isothermal titration calorimetry (1).This degree of inhibition by TFP is followed, in decreasing order, by doxorubicin, promethazine, daunorubicin, amitriptyline, nortriptyline, chlorpromazine, and imipramine. Most of these CSQ-binding drugs showed an inhibition level of ~30 to 40%. In contrast, other compounds that have no binding affinity for CSQ despite their reported major or minor muscle-related side effects, such as ephedrine, theophylline, flunarizine, and dopamine, did not show any significant effect on the SR

calcium contents. Ephedrine, theophylline, dopamine, and the solvent for dissolving a water-insoluble drug, DMSO, showed even slightly increased Ca^{2+} values. In addition to these, various biochemical compounds that have a similar flat multiring structure and molecular weight, such as tetracycline, L-tryptophan, and several smaller-sized molecules such as guanosine, riboflavine, and quinine did not show any significant effect on the total Ca^{2+} content of SR microsome (data not shown).

Concentration and Time Dependence of the Drug Effect on SR Calcium Content: The cCSQ binding drug, TFP, also showed concentration and time dependencies in its effect on total calcium contents of the SR microsome (Figs. 4 and 5). For the concentration dependence study, TFP concentration in the buffer containing microsomes was varied from 10 μM to 1 mM, and as a negative control, the cCSQ non-binding drug ephedrine was used. Figure 4 shows that the microsome incubated for 1 h in a buffer containing 10 μM TFP does not produce any significant difference in calcium content compared with the control SR. However, as the TFP concentration was increased, the calcium content of the SR microsomes was drastically reduced. A similar pattern of TFP concentration dependence was observed for the Ca^{2+}-binding capacity of purified recombinant canine cCSQ (1). As expected, ephedrine, which has no significant affinity to cCSQ, shows no effect on the total calcium content of SR microsome in all concentration ranges tested. For the incubation-time dependence of TFP, SR microsomes were incubated in buffer containing 1 mM TFP for 5, 30, and 120 min. A gradual decrease in calcium content was observed in all samples, possibly caused by long incubation in the presence of continuous mixing the solution with a magnetic stirrer at room temperature. As incubation time increased, the Ca^{2+} content of the SR preincubated with TFP decreased significantly (Fig. 5). After 120-min preincubation with TFP, the SR had almost 50% of the

Ca^{2+} content of the control SR. In the case of ephedrine, the reduction in Ca^{2+} content with increased preincubation time was similar to that of the control SR.

Effect on Calcium Release: As shown in Fig. 6, data using antipyrylazo III and the diode array spectrophotometer indicate that the CSQ binding drug TFP is able to release Ca^{2+} from microsomes (▽), even though the control microsomes continuously take Ca^{2+} from the buffer in the presence of ATP (descending black circle line at the bottom of the figure). By adding a channel blocker for RyR, ruthenium red, we were able to inhibit this drug-induced Ca^{2+} release in a concentration-dependent manner (■ and ◇). Therefore, the TFP-induced release of calcium is, at least in part, thorough the RyR1.

To observe the effect of TFP that is already inside of the SR microsome, each SR microsome was pelleted after incubation with and without TFP for 1 h. The microsomes were further rinsed twice to completely remove the unincorporated TFP. The rinsed pellets were immediately redissolved with calcium-loading buffer, and the calcium-loading experiment was performed as described above. As shown in Fig. 7, the calcium content of the TFP-treated SR was much less than that of the untreated microsome. Even after a 10x calcium load, the SR still did not reach the original calcium level; hence, penetrated TFP molecules result in unrecoverable reduction of the total storage capacity of the SR.

Discussion

Our mass spectroscopy data show that small hydrophobic molecules, such as phenothiazine derivatives, can rapidly diffuse into SR. This behavior among phenothiazine and anthracycline derivatives is consistent with their reported and calculated log *S* (aqueous solubility) and log *P* (partition coefficient) values. Most of these compounds approach the hydrophobic extreme of pharmaceutical drugs (26). Therefore, considering our LC-MS/MS data and previous isothermal calorimetry data (1), those penetrated drugs will be trapped in SR. Given the high concentration of CSQ in SR and the micromolar range affinity between cCSQ and this class of pharmaceutical drugs (1), long-term and/or high-dose administration of these drugs will certainly lead to accumulation of these compounds in the SR. Previously, we showed that the normal Ca^{2+}-binding capacity of purified CSQ is reduced in a concentration-dependent manner by binding to these classes of drugs (1). Therefore, the accumulation of drugs affects both the buffering capacity and the storage level of Ca^{2+} inside of the SR, which is an important determinant of functional activity of RyR.

CSQ serves as a luminal Ca^{2+} sensor through dynamic affinity with the RyR complex. At low Ca^{2+} concentration in the SR, CSQ inhibits the activity of the RyR channel complex through physical interaction. Upon increasing the luminal concentration of Ca^{2+}, this inhibitory interaction is gradually relieved, increasing the probability of channel opening (5; 6; 27)

It is tempting, therefore, to speculate that binding of drugs such as TFP to CSQ weakens the physical interaction between CSQ and the RyR complex, relieving the inhibitory

role of CSQ for the RyR and increasing the opening rate of RyR. In addition, a decreased buffering capacity of CSQ and the luminal SR will result in a higher concentration of the free luminal Ca^{2+} during a period of Ca^{2+} re-entry by the Ca^{2+} ATPase; thereby, a large fraction of RyRs would be in a CSQ-uninhibited mode. This, in turn, accelerates Ca^{2+} discharge.

In this way, exposure to the CSQ-binding drugs can produce a rapid leakage of Ca^{2+}, as observed here and previously (28; 24), and can lower the total Ca^{2+} storage level of the SR in both short- and long-term ways, depending on the level of exposure. We therefore propose that some of the muscle-related side effects among the pharmaceutical drugs, including ones used in this report, from a trembling or shaking to a more serious arrhythmia and sudden cardiac arrest, are the consequence, at least in part, of the interaction between the diffused drugs and CSQ. The reduction of the functional CSQ will produce the same side effects, such as tachycardia, that are observed in the cases of genetic impairment of cCSQ and down-regulation of cCSQ (5).

The exact nature of the conformational change induced by drug binding is still not clear, even though we have proposed a hypothetical model before (1). Elucidation of molecular details will show how certain drugs interact with CSQ and a clear understanding of the underlying regiochemical and stereochemical conformation responsible for drug binding is likely to provide new and global insights into avoiding various types of harmful drug interactions. The studies derived from the corollary hypothesis using SR microsome or CSQ provide not only a potentially simple method for screening drugs but also ideas of how to redesign many pharmaceutical drugs with notorious side effects.

Of course, many reported drug side effects of cardiac or skeletal muscle-related symptoms could have several origins. As noticed herein and in our previous experiments, not all of the drugs with reported muscle-related side effects showed an interaction with cCSQ (1) nor an effect on the calcium-regulating function of the SR.

Noticeably, many endoplasmic reticulum resident proteins such as protein disulfide isomerase and calreticulin, also contain the thioredoxin fold to which every domain of CSQ belongs. These proteins bind Ca^{2+} with low affinity and high capacity, just as CSQ does. Unusual ligand binding activities among these proteins have been reported previously (29; 30; 31; 32)he presence of a thioredoxin fold in these essential regulatory proteins suggests that ligand binding to these proteins may well affect their role in calcium regulation, producing a wide variety of side effects. Therefore, the physiological and biomedical relevance of the adverse interaction between thioredoxin folds and certain classes of drugs is probably very high.

References

1. **Park I., Kim E., Park H., Fields K., Dunker K., and Kang C.** (2005) *Mol Pharmacol*, **67**, 97-104.

2. **MacLennan D., and Wong P. (**1971) *Proc Natl Acad Sci USA*, **68**, 1231-1235.

3. **Park H., Park I-Y., Kim E., Youn B., Fields K., Dunker A., and Kang C.** (2004) *J. Biol.Chem.,* **279**, 18026-18033.

4. **MacLennan D., Abu-Abed N., and Kang C.** (2002) *J. Mol. Cell Cardiol.,* **34**, 897-918.

5. **Terentyev D., Viatchenko-Karpinski S., Gyorke I., Volpe P., Williams S., and Gyorke S.** (2003) *Proc Natl Acad Sci USA*, **100**, 11759-11764.

6. **Beard N., Laver D., and Dulhunty A.** (2004*) Prog. Biophys Mol. Biol.,* **85**, 33-69.

7. **Wang S., Trumble W., Liao H., Wesson C., Dunker A., and Kang C. (**1998) *Nat. Struct. Biol.,***5**, 476-483.

8. **Park H., Wu S., Dunker AK., and Kang C.** (2003) *J. Biol. Chem.,* **278**, 16176-16182.

9. **C., Branden.** (1980) *Q. Rev. Biophys*., **13**, 317-338.

10. **Katti S., LeMaster D., and Eklund H.** (1990) *J. Mol. Biol.*, **212**, 167-184.

11. **He Z., Dunker AK., Wesson CR., and Trumble W.**(1993) *J. Biol. Chem*., **268**, 24635-24641.

12. **Charlier JH., Olson R., Thornock C., Mercer W., Olson D., Broyles T., Muhlestein D., Larson C., Cusack B., and Shadle S.**(2005) *Mol. Pharmacol*., **67**, 1505-1512

13. **Reilly J., Ayis S., Ferrier I., Jones S., and Thomas S. (**2000) *Lancet,* **355**, 1048-1052.

14. **Raehl C., Patel A., and LeRoy M.** (1985) *Clin. Pharm,* **4**.

15. **Witchel H., Hancox J., and Nutt D.** (2003) *J. Clin. Psychopharmacol*., **23**, 58-77.

16. **Jusic N., and Lader M.** (1994) *Br. J. Psychiatry*., **165**, 787-791.

17. **Buckley N, . and Sanders P.** (2000) *Drug Saf.,* **23**, 215-228.

18. **Choi S., Koh Y., and Jo S. (**2005) *J. Pharmacol. Exp. Ther.,* **313**, 888-895.

19. **Olson R., Mushlin P., Brenner D., Fleischer S., Cusack B., Chang B., and Boucek RJ.** (1988) *Proc. Natl. Acad.Sci. USA.,* **85**, 3585-3589.

20. **Zucchi R., and Danesi R.** (2003) *Curr. Med. Chem. Anticancer Agents*, **3**, 151-171.

21. **Szegedi C., Sarkozi S, Herzog A., Jona I., and Varsanyi M. (**1999) *Biochem. J.,* **337**, 19-

22. **Saito A., Seiler S., Chu A., and Fleischer S.** (1984) *J. Cell Biol.,* **99**, 875-885.

23. **Olson R., Li X, Palade P., Shadle S., Mushlin P., Gambliel H., Fill M., Boucek RJ., and Cusack BJ.** (2000) *Toxicol. Appl. Pharmacol.,* **169**, 168-176.

24. **Dachtler M., Handel H., Glaser T., Lindquist D., Hawk RM., Karson CN., Komorsk RA., and Albert K. (**2000) *Magn. Reson. Chem.,* **38**, 951-956.

25. **Walter A., and Gutknecht J.** (1986) *J. Membr. Biol.,* **90**, 207-217.

26. **Gyorke I., Hester N., Jones L., and Gyorke S.** (2004) *Biophys. J.,* **86**, 2121-2128.

27. **Wykovsky W, Hauptner R, and Suko Drug-induced calcium release from heavy sarcoplasmic reticulum of skeletal muscle. (**1988) *Biochim. Biophys. Acta ,* **938**, 89-96.

28. **Nigam S., Goldberg AL., Ho S., Rohde MF., Bush KT., and Sherman MYu.** (1994) *J. Biol. Chem.,* **269**, 1744-17.

29. **Michalak M., Mariani P., and Opas M .** (1998) *Biochem. Cell Biol*., **76**, 779-785.

30. **Ferrari, D. and Soling, H.** (1999) *Biochem. J.,* **339**, pp. 1-10.

31. **Corbett E., Michalak KM., Oikawa K., Johnson S., Campbell ID., Eggleton P., Kay C., and Michalak M.** (2000) *J.Biol. Chem*., **275**, 27177-27185.

Table1. TFP quantification in SR pellet after incubation with 1 mM TFP through LC-MS/MS

Sample	TFP amount
SR peSR pellet after TFP incubation	1.02 ± 0.02 μg of TFP/mg of SR pellet
SuperSupernatant after ultracentrifugation	11 ± 2 μg of TFP/ml of supernatant
SR peSR pellet after rinsing with a fresh buffer	0.75 ± 0.05 μg of TFP/mg of SR pellet
SuperSupernatant after reultracentrafugation	1.4 ± 0.2 μg of TFP/ml of supernatant

Table2. ***Ca^{2+} Capacity of SR (%) after incubating with drugs and 10times (7nmol) Ca^{2+} loading***

Rabbit Skeletal Sarcoplasmic Reticulum(33mg/ml) dissolved in a buffer solution (20mM MOPS(pH 7.5), 50mM KH_2PO_4, 5mM KCl, 2mM $MgCl_2$, 2mM ATP) was incubated with 1mM of each drug for 1hr and titrated with7nmol of $CaCl_2$ 10times. Ca2+ Capacity was measured through Atomic Absorption Spectroscopy. Ca^{2+}Capacity of only Ca^{2+} added SR is 100%.

Drugs	Ca2+ Capacity of SR (%)
Original SR	77.94
Ca2+ added SR	100
Ephedrine	100.58
Theophyline	100.88
Flunarizine	97.37
Dopamine	100.08
Tetracycline	93.94
DMSO	102.0
L-Tryptophan	92.39
Imipramine	67.07
Daunomycine	61.75
Doxorubicin	61.02
Chlorpromazine	64.07
Nortriptyline	62.5
Amitriptyline	62.16
Trifluoperazine	59.75
Promethazine	61.42

Fugure legends

Fig. 1 A, Representative tracing of the process of loading SR microsomes with Ca^{2+}. The metallochromic indicator, antipyrylazo III, was used to monitor calcium uptake by measuring differences in absorbance (A_{710}–A_{790}), using an HP8452A UV/Vis diode-array spectrophotometer.

B, The amount of calcium in SR microsomes at each $CaCl_2$ loading step. With continuous mixing, 7 nmol of $CaCl_2$ was added to the 1-ml buffer solution containing ~5 mg SR microsomes. After 5 min of each loading, the SR solution was ultracentrifuged, and the amount of Ca^{2+} was measured through Atomic Absorption Spectrophotometer (Shimadzu) at the absorption wavelength of 422.7 nm.

Fig. 2, Mass spectroscopic data. MS/MS product ion spectrum of TFP (100 nM) under the conditions of the analysis, showing fragments of the protonated parent ion selected by Q1 (408.1 *m*/*z*, entirely consumed in collision process). Calibration of TFP by LC-MS/MS was done in selective reaction monitoring mode.Mass spectroscopic data.

Fig. 3, Inhibition effect of certain drugs that have muscle-related side effects. SR microsomes were incubated in a buffer containing each drug and were loaded 10 times with Ca^{2+}. The Ca^{2+} content for each sample was measured through atomic absorption spectroscopy. Data are expressed as a percentage of the amount of Ca^{2+} in drug-untreated SR microsome. SR, original SR microsome without any Ca^{2+} or drug; Ca^{2+}, Ca^{2+} loaded SR microsome without any drug; EPR, ephedrine; TPL, theophylline; FLZ, flunarizine; DP, dopamine; TC, tetracycline; L-TTP: L-tryptophan; IPR, imipramine; DAUN, daunorubicin,

DOXO, doxorubicin, CPMZ, chlorpromazine; NRT, nortriptyline; AMT, amitriptyline; TFP, trifluopromazine; PMZ, promethazine.

Fig. 4, Concentration dependence of TFP inhibitory effect. SR microsomes were incubated in the presence of TFP and ephedrine before the addition of Ca^{2+}. The concentrations of two drugs were varied from 0.01 to 1 mM.

Fig. 5, Time dependence of TFP. Total calcium contents were measured for SR microsomes that were incubated in a loading buffer containing 1 mM concentration of TFP or ephedrine for 5, 30, and 120 min.

Fig. 6, Calcium release effect of TFP. For the upper trace (▽), TFP (0.2 mM final concentration) was added to SR microsomes after the 10th loading of Ca^{2+}. The bottom trace (●) shows absorbance changes after the addition of the 10th loading of Ca^{2+}. The two middle traces show absorbance changes after the 10th loading of Ca^{2+} followed by addition of ruthenium red and TFP, with final concentrations of 10 μM (■) and 20 μM (◇), respectively, and 0.2 mM TFP.

Fig. 7, The effect of absorbed TFP. SR microsomes were incubated for 1 h in a loading buffer containing 1 mM concentration of TFP. Then they were centrifuged and rinsed twice to remove the unincorporated TFP, and the pelleted SR microsomes were redissolved in fresh buffer without TFP. While continuously mixing the solution with a magnetic stirrer, Ca^{2+} was loaded 10 times by adding 7 nmol of $CaCl_2$ solution each time, which elevated the calcium concentration of the solution to 70 nM. Original SR, SR without any Ca^{2+} or drug treatment; TFP, TFP preincubated SR without Ca^{2+} loading; TFP + 10 Ca^{2+}, TFP preincubated and 10 times Ca^{2+} loaded SR; 10 Ca^{2+}, 10 times Ca^{2+} loaded SR.

Fig. 1 A

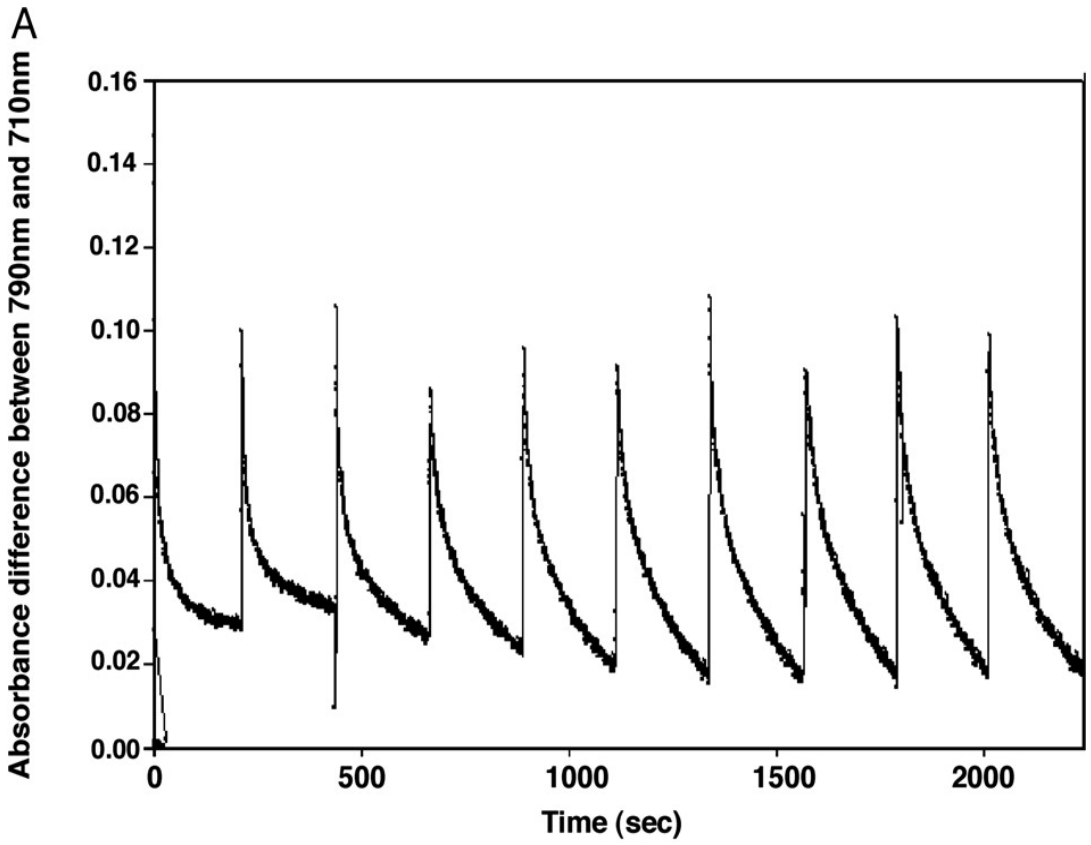
A
Absorbance difference between 790nm and 710nm
0.16
0.14
0.12
0.10
0.08
0.06
0.04
0.02
0.00
0
500
1000
1500
2000
Time (sec)

Fig. 1 B

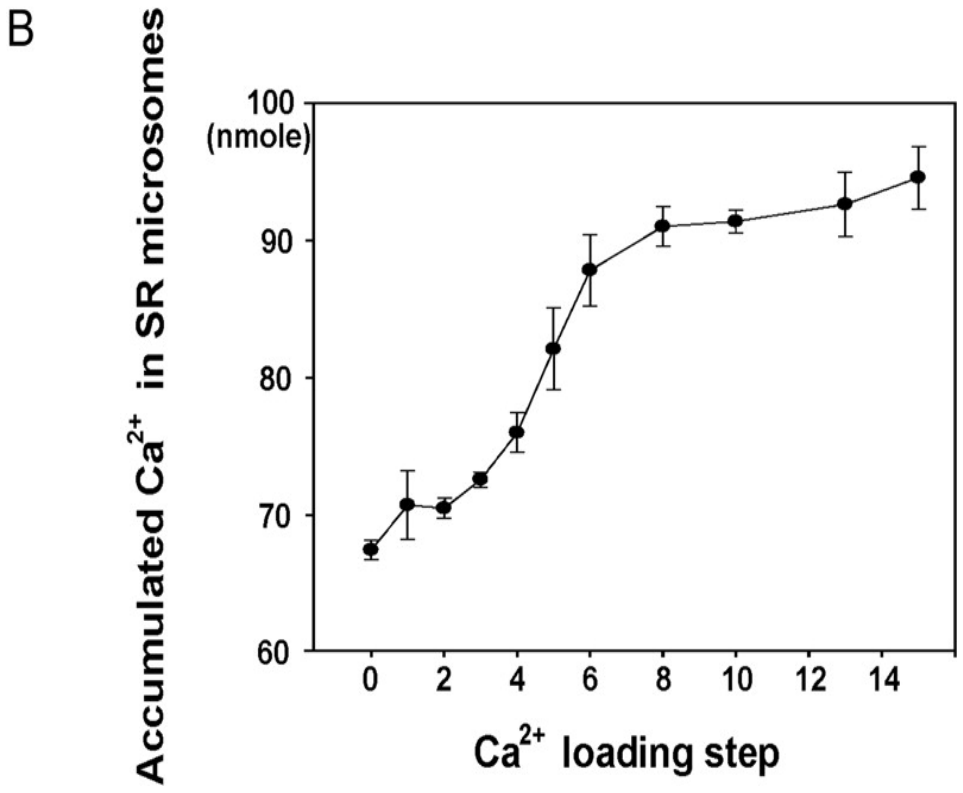
B
Accumulated Ca2+ in SR microsomes
100
(nmole)
90
80
70
60
0
2
4
6
8
10
12
14
Ca2+ loading step

Fig. 2

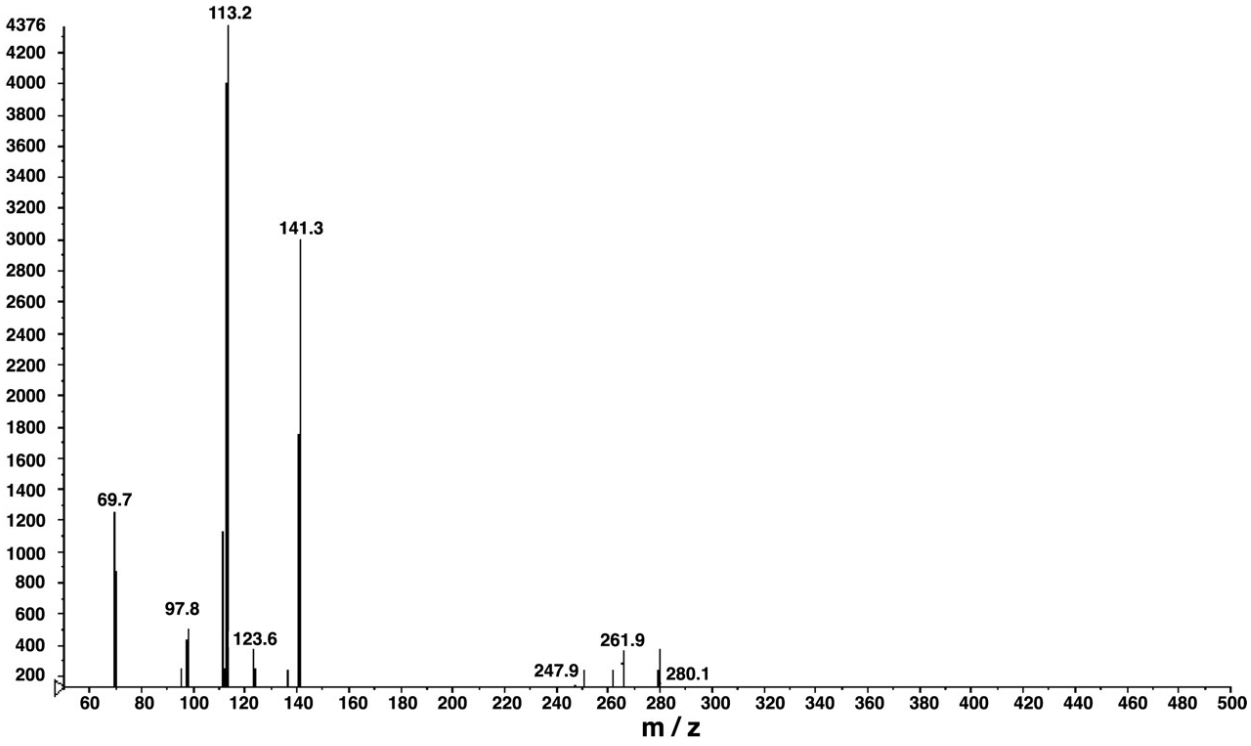

Fig. 3

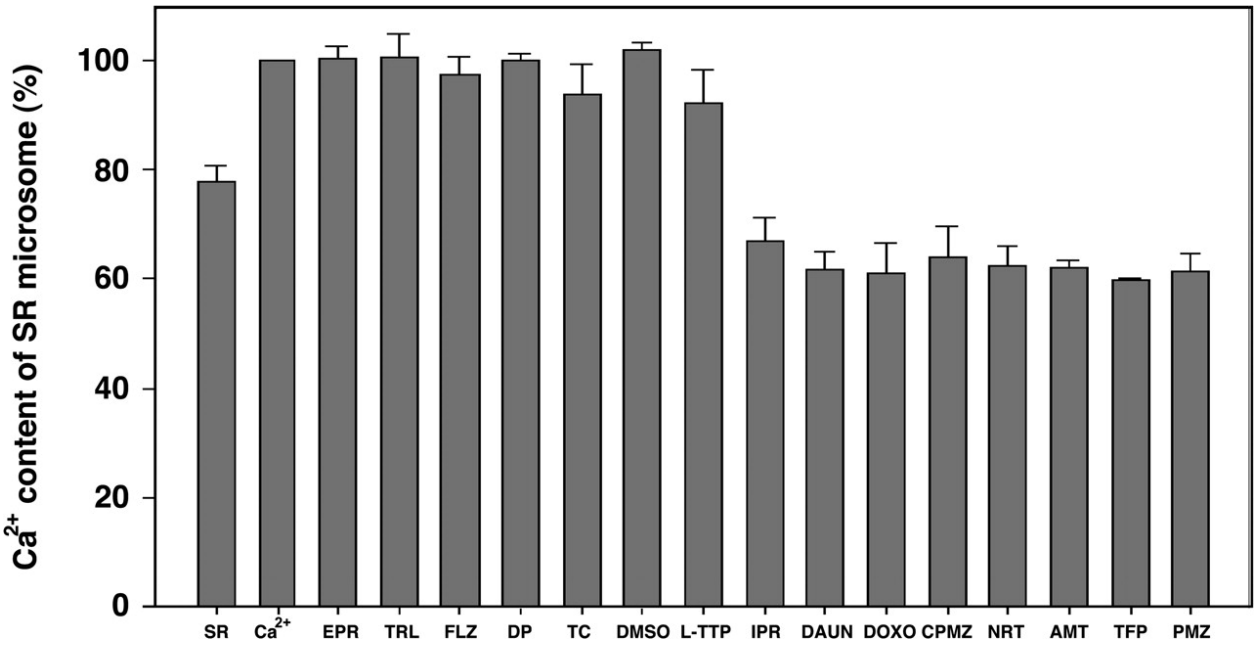
Ca2+ content of SR microsome (%)
0
20
40
60
80
100
SR
Ca2+
EPR
TRL
FLZ
DP
TC
DMSO
L-TTP
IPR
DAUN
DOXO
CPMZ
NRT
AMT
TFP
PMZ

Fig. 4

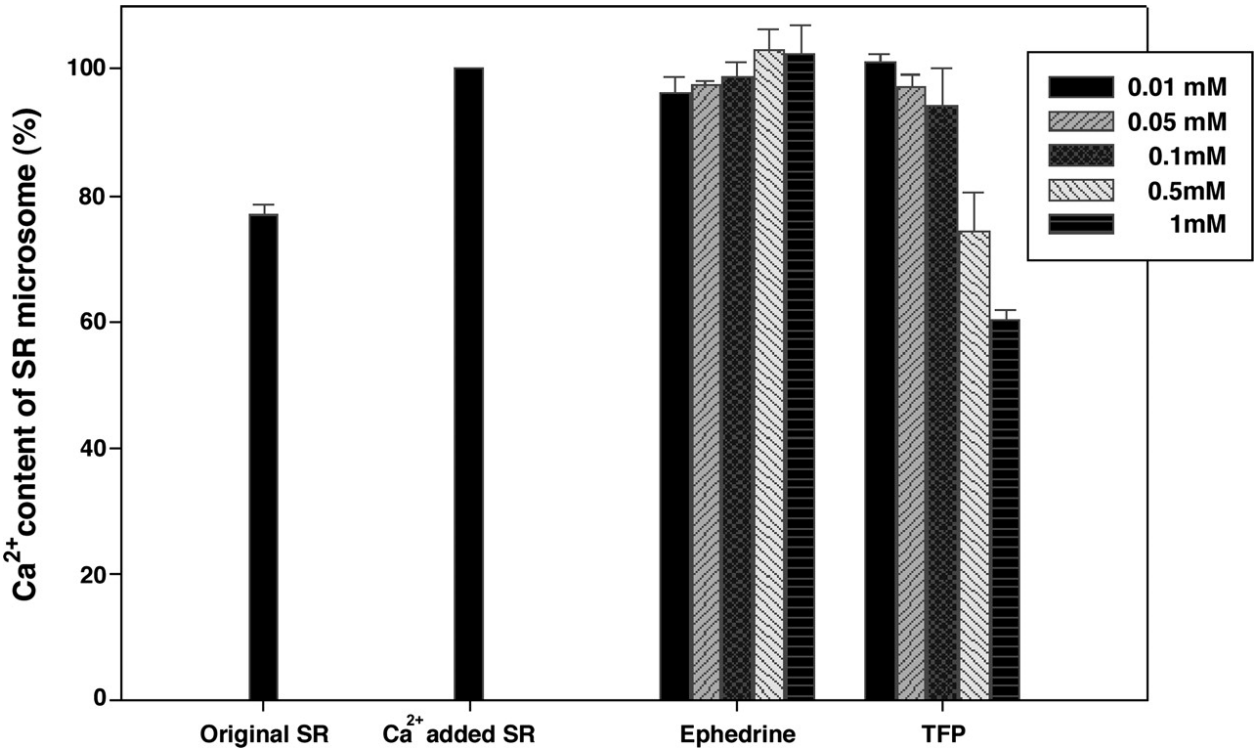
Ca2+content of SR microsome (%)
0
20
40
60
80
100
Original SR
Ca2+ added SR
Ephedrine
TFP
0.01 mM
0.05 mM
0.1mM
0.5mM
1mM

Fig. 5

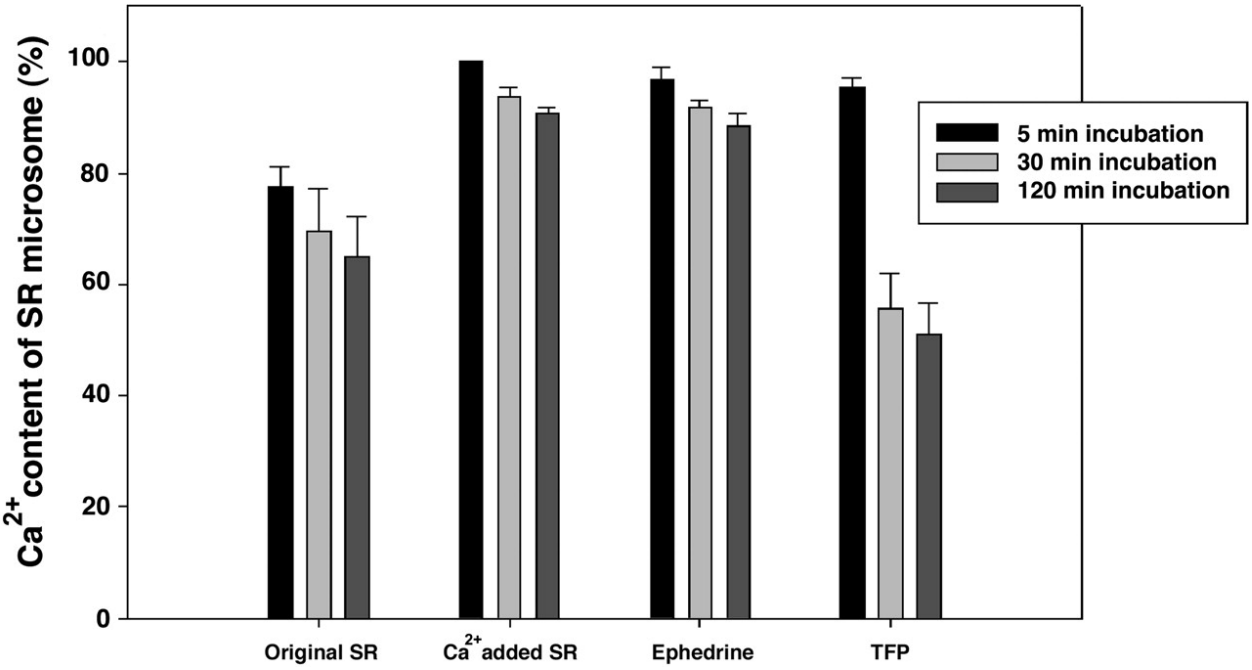
Ca2+ content of SR microsome (%)
100
80
60
40
20
0
Original SR
Ca2+ added SR
Ephedrine
TFP
5 min incubation
30 min incubation
120 min incubation

Fig. 6

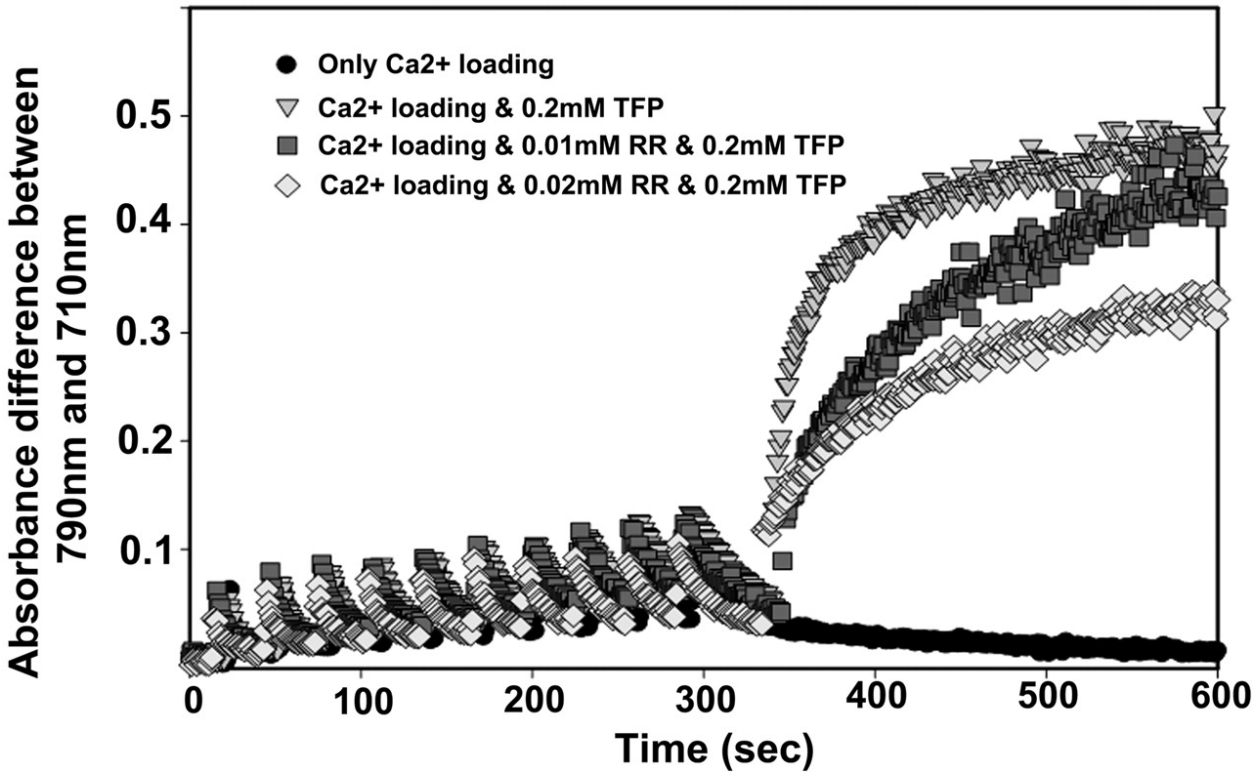
Only Ca2+ loading
Ca2+ loading & 0.2mM TFP
Ca2+ loading & 0.01mM RR & 0.2mM TFP
Ca2+ loading & 0.02mM RR & 0.2mM TFP
Absorbance difference between 790nm and 710nm
0.1
0.2
0.3
0.4
0.5
0
100
200
300
400
500
600
Time (sec)

Fig. 7

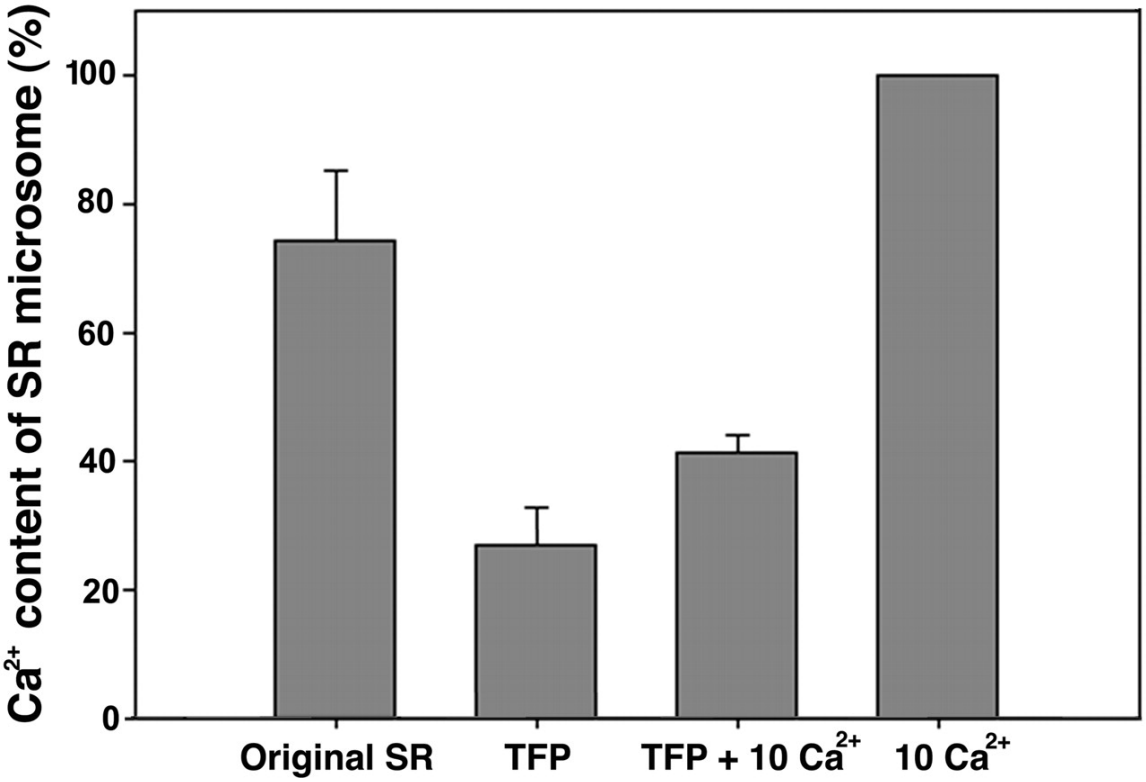
Ca2+ content of SR microsome (%)
100
80
60
40
20
0
Original SR
TFP
TFP + 10 Ca2+
10 Ca2+

CHAPTER TWO

BIOCHEMICAL ANALYSIS OF HUMAN CARDIAC CALSEQUESTRIN AND ITS DELETERIOUS MUTANTS

Preface

The sarcoplasmic reticulum (SR) plays an essential role in muscle excitation-contraction coupling by regulating the cytosolic free Ca^{2+} concentration. One of the main SR proteins responsible for this Ca^{2+} regulation is the Ca^{2+} storage protein, Calsequestrin (CSQ). Catecholaminergic Polymorphic Ventricular Tachycardia(CPVT) is a rare arrhythmogenic disorder characterized by syncopal events and sudden cardiac death at a young age without any structural heart problem. It has been reported that several mutations (R33Q, L167H, D307H) in the human cardiac CSQ are related to CPVT but the precise molecular mechanisms are still poorly understood.

In this manuscript, we investigated the effects of the various CPVT-related CSQ mutations on Ca^{2+} binding capacity, polymerization and conformational changes to understand the effect of CSQ altered function on CPVT development. From the applied biochemical and biophysical experiments, it was shown that these CSQ mutations resulted in decreased Ca^{2+} binding capacity and altered [Ca^{2+}] dependency of the CSQ polymerization, which is the most important feature of CSQ for high Ca^{2+} binding capacity. Compared to wild type CSQ, the mutated CSQ showed a different polymerization pattern at the same [Ca^{2+}]. Therefore, it was suggested that the mutated CSQ in CPVT patients can be involved in the disruption of Ca^{2+} regulation in SR, and this seems as the major cause of CPVT development.

The following manuscript will be submitted to *Journal of Biological Chemistry* in May 2007.

Biochemical analysis of human cardiac calsequestrin and its deleterious mutants

EunJung Kim[1], Buhyun Youn[1], Lenord Kemper[2], Cait Campbell[1], Magdolna Varsanyi[3], and ChulHee Kang[1,2]*

From the [1]School of Molecular Biosciences, Washington State University Pullman, [2]WA 99164-4660, Department of Pharmaceutical Sciences, Washington State University Pullman, WA 99164-6534 and [3]Institut für Physiologische Chemie, Ruhr Universität, D-44780 Bochum, Germany

*Address correspondence to: ChulHee Kang, School of Molecular Biosciences, Washington State University, Pullman, WA 99164-4660; Tel. 509-335-1409; Fax. 509-335-9688; Email: chkang@wsunix.wsu.edu

Summary

Mutations of highly conserved residues of human cardiac calsequestrin (cCSQ), a high capacity and low affinity calcium binding protein in the sarcoplasmic reticulum, have been associated with the pathophysiologic event, catecholaminergic polymorphic ventricular tachycardia (CPVT). In order to understand the molecular mechanism and pathological link between these CPVT-related missense mutations of CSQ and the resulting arrhythmias, we generated the CPVT-causing mutants of human cCSQ (R33Q, L167H, D307H) and two pathophysiologically null mutants (T66A and V76M) and investigated the effect of these mutations on CD and fluorescence spectra, calcium binding, Ca^{2+}-dependent polymerization and binding affinity to junctin. In addition, we determined the crystal structure of the corresponding wild-type human cCSQ to gain insight into the structural effects of the mutations. Based on the 4Å resolution crystal structure and the structure of canine cCSQ, we mapped the corresponding mutations and explained their altered behaviors. All three CPVT-related mutations are located at a place that can perturb the local structure.

Our data show that all three CPVT-related mutations lead to severe changes in both K^+-dependent fluorescence spectra and Ca^{2+}-binding capacity in spite of the similarity of their CD spectra to that of the wild-type human cCSQ. In addition, light-scattering and cross-linking experiments also indicate that the calcium-dependent monomer-polymer transitions of the mutants are quite different compared to those of wild-type. One of the pathophysiologically null mutants, T66A shows very similar characteristics with the wild-type. But the other null mutant, V76M, shows significantly altered behavior, even though it is

less severe compare to those of three CPVT-related mutants, calling for careful reconsideration of its status.

FOOTNOTES AND ABBREVIATIONS

This work was supported by National Science Foundation (MCB-0117192), the American Heart Association, and the Murdock Charitable Trust.

The abbreviations used are:

CSQ: calsequestrin*,*

SR: sarcoplasmic reticulum,

ITC: isothermal titration calorimetry,

ADR: adverse drug reaction,

K_d*: dissociation constant,*

E-C: excitation-contraction,

TCA: tricyclic antidepressants,

RyR: ryanodine receptor

Introduction

Catecholamine-induced polymorphic ventricular tachycardia (CPVT) is a familial arrhythmogenic disorder characterized by syncopal events, seizures or sudden cardiac death at a young age(1-4). CPVT patients, who usually do not show any detectable cardiac disease, manifest ventricular premature beats and PVT in response to exercise or on exposure to catecholamines (1). Although the very high mortality rate amounting to 30 to 35% by the age of 30 years (5), calls for effective preventive measures (6), sudden death seems to constitute the first manifestation of this disease (7).

CPVT seems to be caused by the aberrant release of Ca^{2+} from the sarcoplasmic reticulum (SR), which triggers early and delayed after-depolarizations (DADs) and extrasystolic Ca^{2+} waves(1,8,9). Therefore, the disease can be linked naturally to a defective RyR itself or other malfunctioning regulatory components of the channel gating machinery. Mutations in the cardiac ryanodine receptor 2 (RyR2) are known to cause the autosomal dominant form of this CPVT(10-13). In addition, mutations of cardiac calsequestrin (cCSQ) have been suggested as the cause of an autosomal recessive or dominant form of CPVT (2,6,14,15). So far, three missense mutations and a deletion mutation in highly conserved regions of the cCSQ gene have been found among severe inherited CPVT patients in autosomal recessive forms (http://www.fsm.it/cardmoc/) (14,15), suggesting that mutations in cCSQ are more common than previously thought (2,16,17).

The 40 kD CSQ acts as a major Ca^{2+} storage or buffer protein within the sarcoplamic reticulum (SR) of both cardiac and skeletal muscle during excitation-contraction coupling processes, thereby lowering free Ca^{2+} concentrations and facilitating further uptake by the

Ca^{2+}-ATPases. CSQ binds Ca^{2+} ions with high capacity (60-80 mol Ca^{2+} mol^{-1} CSQ), but moderate affinity (Kd=1mM) over the physiological range of Ca^{2+} concentration and releases it with a high off rate (18,19). Not only does CSQ act as a Ca^{2+} buffer, but also CSQ actively participates in muscle contraction by localizing Ca^{2+} at the release site and regulating the amount of Ca^{2+} released through the RyR channel (20). In addition, CSQ modulates the luminal Ca^{2+}-dependent closure of the RyR, thus CSQ determines the functional size and stability of SR Ca^{2+} stores (5,21).

The unique and high capacity Ca^{2+}-binding property of CSQ is initiated by the formation of Ca^{2+}/CSQ complexes at relatively high CSQ and Ca^{2+} concentrations (22). Under such conditions, two-thirds of the total bound Ca^{2+} is associated with Ca^{2+}/CSQ polymers, while one-third is associated with the soluble forms of CSQ molecules. The Ca^{2+}/CSQ polymers or aggregates are easily dissociated by K^{+}, which lowers the affinity of Ca^{2+} for CSQ (19,23-29). Ca^{2+}-induced CSQ precipitation leads to fibrils or needle-like crystals (30-32). Likewise, electron microscopy reveals fibrous arrays in the SR at the junctional membranes, and these arrays are believed to be CSQ in its Ca^{2+}-bound form (30,33,34). Cross-linking studies also demonstrate that most CSQ in the SR are involved in CSQ/CSQ complexes, reflecting the physiological relevance of these CSQ polymers (28,35,36).

CSQ delivers its effect through interaction with junctin and triadin, which appears to stabilize CSQ at the inner face of the junctional SR membrane (37-41). As expected, overexpression of junctin and triadin has been already associated with CPVT pattern (42). The N-terminal regions of these proteins are located in the cytoplasm and their C-terminal regions are located in the lumen of the SR. The luminal domain of these proteins, which is

highly enriched in charged amino acids organized into "KEKE" repeats, have been proposed to bind directly to CSQ (39,41,43). All together, these data suggest that there exists a quaternary protein complex of RyR, CSQ, triadin and junctin, allowing CSQ to sequester Ca^{2+} in the vicinity of the RyR during Ca^{2+} uptake and release, assuring the high concentrations of Ca^{2+} being stored very near to the site of Ca^{2+} release (44). A detailed mechanism whereby certain mutations of cCSQ induce CPVT remains to be elucidated.

Here we report on the crystal structure of wild-type human cCSQ (HcCSQ) and the functional characteristics of three CPVT-related mutants, R33Q, L167H and D307H. In addition, two pathologically null mutants, T66A and V76M, which show an equal polymorphism among patients and normal people, were investigated. We conducted detailed comparisons of these mutants with wild-type CSQ, including differences in secondary structures, calcium binding capacity, Ca-dependent polymerization and binding to the junctional SR membrane protein, junctin.

EXPERIMENTAL PROCEDURES

Expression and Purification of Calsequestrins and Junctin— Wild type human cardiac calsequestrin (HcCSQ) with NcoI and XhoI sites was subcloned into pET28a after removing the sequence region of the signal peptide and then transformed into *E.coli* BL21 (DE3). Cells were grown in Luria Bertani (LB) media containing kanamycin 30μg/ml until the OD_{600} reached 0.8 at 37 °C, then 0.5mM IPTG was added to start induction at 30 °C for 10 hours. In order to generate five CPVT-related human cCSQ mutants (R33Q, T66A, V76M, L167H, D288H), a QuikChange XL Site-Directed Mutagenesis Kit (Stratagene, La Jolla, CA) was used and the resulting mutations were confirmed through DNA sequencing. All five mutants were transformed into the *E.coli* strain, ER2566, and overexpressed under the same conditions as the wild-type. For the expression of a truncated junctin, canine cardiac junctin containing SalI and XhoI sites was introduced into pET24b and transformed into *E. coli* strain, ER2566. Cells were grown in YEP (10g of Yeast extract and 20g of Bacto peptone 20g in 1L) media containing kanamycin 30 μg/ml, until the OD_{600} reached 0.8 at 37 °C, then protein induction was performed by lowering the temperature to 30 °C and adding 0.5mM IPTG. Cells were, then, allowed to grow further for 10 more hours.

For purification of wild-type and mutant HcCSQs, DEAE (TOYOPEARL, DEAE-650M, TOSOH Bioscience LLC) was used initially to purify the proteins. After harvesting the cells, they were sonicated (5 x 10 s, model 450 Sonifier®, Branson Ultrasonics), in Buffer A (20mM Tris-HCl, pH 7.0), followed by centrifugation at 20,000g for 40 minutes. After centrifugation, the supernatant was injected into the DEAE column and HcCSQ proteins were eluted with a linear gradient between Buffer A (20mM Tris-HCl, pH 7.0) and Buffer B

(20mM Tris-HCl, pH 7.0, 2M NaCl). The wild-type and mutant cCSQs were eluted between 400 - 600mM NaCl. The fractions containing HcCSQ were removed and transferred to an Amicon concentrator (membrane cutoff 10kD). The buffer was then changed to Buffer C (5mM sodium phosphate, pH 6.8) for the CHT-10-I Hydroxy apatite (HA, BioRad, Hercules, CA) column. Human cCSQs were eluted from ~300mM sodium phosphate (pH6.8) between Buffer C and Buffer D (500mM sodium phosphate, pH 6.8). Fractions containing HcCSQs were concentrated, followed by a buffer exchange with Buffer A for the MonoQ column (Amersham Biosciences GL10/100). The proteins were allowed to elute through a step gradient from 0 to 2M NaCl (Buffer B). Wild type and mutant human cCSQs were eluted between 400 and 600mM NaCl.

For the purification of junctin, cells were sonicated in a wash buffer (50mM NaH_2PO_4, 300mM NaCl, 20mM imidazole pH8.0), followed by centrifugation at 20,000g for 40 minutes. The supernatant was injected into the pre-equilibriated Ni-NTA (Qiagen) column with wash buffer and the column was washed with 15 column volumes of the wash buffer followed by protein elution. The elution buffer contained 50mM NaH_2PO_4, 300mM NaCl and 250mM imidazole with a final pH 8.0.

Fluorescence Spectroscopy and Circular Dichroism — For the intrinsic fluorescence emission spectra, 0.02mg/ml of wild-type and mutant proteins, in 10 mM MOPS (pH 7.2) and KCl ranging from 0 to 600 mM, was used to assess the K^+ dependent fluorescence changes. Measurements were performed with an AVIV spectrofluorometer (AVIV Biomedical, Inc.) at 25 °C. Each protein was excited at 295 nm using 1nm bandwidth with a photomultiplier voltage setting of 620V. Emission was scanned from 310 to 400nm using 2nm bandwidth. CD spectra were measured with an AVIV spectropolarimeter (AVIV

Biomedical, Inc.) at 25 °C. 0.35mg/ml of protein was buffered in 10 mM MOPS (pH 7.2) with 300 mM KCl. Spectra were recorded from 200 to 260 nm.

Equilibrium Dialysis and Atomic Absorption Spectrophotometry— To prepare the proteins for equilibrium dialysis, approximately 2.5 mg/ml of purified wild-type and individual mutant HcCSQ proteins were extensively dialyzed for 3 days in distilled water. The dialysis solution was then switched to a buffer containing 10mM Tris-HCl (pH 7.5), 300mM KCl and 2mM NaN_3 and dialysis was performed continuously for 1 week under refrigerated conditions with a constant reservoir buffer change in every 24 hours. Dialyzed proteins and various concentrations (1 to 25mM) of calcium chloride standard solution (Fluka chemika) were applied to the half-cell of a modified horizontal diffusion chamber. One ml of protein and the calcium chloride solutions in each chamber were equilibrated against each other for 36 hours on a rocking shaker at room temperature. The total bound calcium concentrations of wild-type and individual mutant HcCSQ were analyzed using an Atomic Absorption Spectrophotometer (Shimadzu AA-6200) at the analysis line wavelength of 422.7nm. After equilibrium dialysis, protein and calcium solutions from each cell were diluted to bring their corresponding calcium concentrations within the detection range. Calcium concentration was determined after calibrating the instrument with a series of calcium chloride standard solutions. Protein concentration of each dialysis cell was measured by the Bradford assay. Fractional occupancy (Y= [bound calcium]/[total CSQ]) was calculated as the difference in Ca^{2+} concentrations between two compartments.

Cross-linking Experiments— 1.5mg/ml protein in 150mM KCl, 20mM HEPES pH7.5, 2mM $CaCl_2$ was mixed with the cross-linking buffer containing 100mM sodium phosphate pH7.5, 150mM NaCl and dithiobis-sulfosuccinimidyl-propionate (DTSSP) to a final

concentration of 0.1mM. The mixture was then incubated on ice for 2 hours. After incubation, the cross-linking reactions were quenched by the addition of Tris-HCl (pH 7.5) to a final concentration of 50mM. Samples were, then, mixed with 2x SDS sample buffer without DTT and were run using a premade linear gradient SDS-PAGE (Ready Gel 4-20% Tris-HCl, Biorad).

Light Scattering: — The wild type and five mutant proteins, at a concentration of 1.6mg/ml in 300mMKCl, 10mM Tris-HCl (pH 7.5), 1mM DTT, were equilibrated at room temperature for 30 minutes before injecting into the size-exclusion column (Shodex PROTEIN KW-803, Shodex Inc.). 100µl of each protein was injected and the chromatography was carried out at a 1ml/min flow rate using an Acuflow series IV pump (Analytical Scientific Inst.). The sample was passed through an UV detector (SSI 500 Variable UV/Vis, Scientific Systems Inc.), a refractometer (Optilab DSP, Wyatt Tech.), and a multi-angle laser light-scattering detector (Dawn EOS, Wyatt Tech.). The experiments were performed at room temperature.

Crystallization and Structure Determination— For crystallization, a solution of purified HcCSQ (7mg/ml) in 20mM Tris-HCl (pH 8.5) containing 1mM DTT, 1mM EDTA and 400mM NaCl. Crystallization trials were performed using the hanging drop vapor diffusion method at two temperatures (277 and 293 K). Optimized HcCSQ crystals were obtained at 277 K by mixing the 2.0 µL of above protein solution with a 1.5 µL of reservoir solution containing 2M sodium chloride and 10% (w/v) PEG 6000. After 1-2 days, square shaped crystals were noted and growth was monitored for two weeks. HcCSQ belongs to the space group $I4_122$ with unit cell dimensions of a = b = 150.65Å, c = 227.47Å with one molecule per asymmetric unit. For X-ray diffraction studies, single crystals were transferred

into solutions of cryoprotectant (25% glycerol in each reservoir solution) through three solutions with intermediate concentrations of these reagents and quickly frozen and stored in liquid nitrogen until data collection. Diffraction data was collected at the Berkeley Advanced Light Source (ALS, beam line 8.2.1) at 100K. Data were indexed, integrated, and scaled with CrystalClear 1.3.6 (Rigaku MSC). The structure of HcCSQ was determined by molecular replacement using the coordinates of the previously determined crystal structure of wild-type canine cCSQ (1SJI). After rigid refinement with resolutions of 15 and 4.5 Å, the R-value was determined to be 31.12%. The final R-factors was 23.7% (R_{free} = 27.6% for the random 5% data). The number of reflections above 2σ level was 4,119 (90.7% completeness) between 25.0 and 4.0 Å resolution. The root mean square deviations (r.m.s.d.) (from ideal geometry) of the final coordinates are 0.02 Å for bonds and 3.3º for angles, respectively. The coordinates have been deposited in the Protein Data Bank.

RESULTS

Far UV Circular Dichroism and Fluorescence Spectra: Three recombinant proteins representing CPVT-related missense human cCSQ mutants (R33Q, L167H, D307H) and two known pathological null mutants (T66A, V76M) were cloned and purified (Fig. 1 inset). The structural integrity of the purified CPVT-related mutant proteins was checked and compared with the wild-type hcCSQ by measuring their CD spectra (Fig.1). As shown in the figure, the patterns of the spectra in a buffer containing 300mM KCl were very similar to that of wild-type. They all have two negative bands around 208 and 222 nm, which are the characteristics of CD spectra of typical α-rich or αβ proteins. L167H shows the least similarity in terms of depth of its minima.

Fig. 2A shows the change in the intrinsic fluorescence of the wild-type and mutants as K^+ concentration increases. In this experiment, the protein concentrations of all HcCSQs were adjusted to the same level by monitoring their UV absorbances at 280 nm. In Fig. 2B, to ease comparison among proteins, the relative responses to [K^+] change, instead of absolute emission values, were plotted (45). That is, the absolute value of fluorescence at 330 nm in the absence of K^+ was adjusted to 1.0 and their relative changes of fluorescence were plotted as a function of [K^+]. As shown in both Fig. 2A and 2B, the K^+-dependent fluorescence changes for wild-type and T66A share a very similar pattern and their amounts of fluorescence emission are very similar. On the other hand, V76M shows a slightly different response to the K^+ increase and the emission amount is lower than those of wild-type and T66A mutant, even though it reportedly has no physiological effect. All three CPVT-related

mutants, especially L167H and D307H, (46) show little K^+-dependent response. In addition, the D307H shows significantly lower fluorescence emission than the other proteins.

The effect of mutation on calcium binding capacity of cCSQ: In order to monitor any change in the Ca^{2+} binding capacities of the CPVT-related mutants and the non-pathological mutants, relative to the wild-type hcCSQ, their Ca^{2+} binding capacities were measured by equilibrium dialysis and atomic absorption spectroscopy. The proper buffer condition for measuring the Ca^{2+} binding was chosen based on our previous circular dichroism (CD), fluorescence spectroscopies and light scattering experiments (28). The molecular weight estimate from light scattering data for the CSQ at this condition is approximately 44 (±1)kD, corresponding closely to the monomeric CSQ (28).

As shown in Fig. 3, calcium binding capacity of the pathological null mutant, T66A, roughly matched that of the wild-type along the entire range of Ca^{2+} concentration tested by equilibrium dialysis. Both wild-type and T66A HcCSQ reach approximate values of 12 - 13 bound Ca^{2+} at 1mM. At 5mM $CaCl_2$ concentration, the Ca^{2+} binding capacities of those two reach the level of ~20. But another null mutant, V76M shows a slightly diminished binding capacity. Both wild-type, T66A and V76M hcCSQs show sharp increases in their Ca^{2+} binding capacities between 0 and 1mM Ca^{2+} concentration, even though V76M lags behind (Fig. 3). Our data also clearly show a significant decrease in the Ca^{2+} binding capacities for all three CPVT-related mutants, R33Q, L167H and D307H. In particular, the L167H mutant shows approximately 50% capacity compared to that of wild type across the range of the Ca^{2+} tested.

The effect of mutation on Ca^{2+}-dependent polymerization of HcCSQ: We monitored the size exclusion chromatography elution profiles for wild-type and CPVT-related mutant cCSQs using multi-angle laser light scattering (690 nm) and differential refractometry (DAWN-EOS and Optilab, Wyatt Technology Corp.), which allows the determination of molecular weights across chromatographic peaks. At a K^+ concentration of 300mM without any Ca^{2+} ion, the major portion of the wild-type hcCSQ eluted in a monomeric form and a small fraction of the protein eluted in a dimeric form. The addition of Ca^{2+} at the final concentration of 1mM resulted in transition of the major fraction from monomer to dimer. The T66A mutant cCSQ shows very similar pattern of elution in both conditions, but all three CPVT-related mutants and even V76M show quite different patterns in both conditions. Both R33Q and D307H do not exhibit the same Ca^{2+}-dependent response of the wild-type, even though they show a trend of increased amount of dimer peaks in response to the Ca^{2+} ion. Instead they continuously maintain a large portion of their monomer population even in the presence of 1mM Ca^{+2}. The L167H mutant exhibits the largest shift from the elution pattern of the wild-type. Not only it does not show any Ca^{2+}-dependent response observed in the wild-type cCSQ and T66A mutant, but it also shows various heterogenous peaks of high molecular weight even in the 300mM KCl containing buffer solution. Our chemical cross-linking experiments with dithiobis-sulfosuccinimidyl-propionate (DTSSP) (Fig. 4) also show polymerization patterns in cation-dependent manners, which agrees with the light scattering result (Fig. 5). Concentrations of CSQ and DTSSP, reaction time and acrylamide concentration for PAGE gels followed our previous optimized conditions for canine cCSQ.

Crystal Structures of hcCSQ: The asymmetric unit of crystalline canine cCSQ has one independent molecule. In the crystal lattice, the HcCSQ monomers stack with alternating orientations forming a continuous ribbon-like linear polymer of ~90Å thick defining two different types of packing interfaces, front-to-front and back-to-back (Fig. 6A). The 13 highly extended, N-terminal residues of one cCSQ monomer lie along a hydrophobic cleft between two β-strands of domain II of the neighboring symmetry-related cCSQ monomer (arm exchange or domain swapping).

The overall structure of human cCSQ is composed of three nearly identical thioredoxin-like domains (Fig 6B). Each individual domain has a five-stranded β-sheet with two α-helices in both sides, composed of approximately 100 residues (residues 22-142, 143-246, 247-370). Every domain has a highly conserved hydrophobic core with acidic residues on the exterior, generating highly electronegative potential surfaces. Two N-terminal residues and 29 C-terminal residues starting from Asn371 are disordered and the corresponding electron densities for these regions are not visible.

DISCUSSION

Overall, the 3D-structure of human cCSQ, which has three identically folded thioredoxin domains, is very similar to that of canine cCSQ. The individual domain of human cCSQ contains a high net negative charge, ranging from about -8 to –23. In addition, the disordered C-terminal tail of human cCSQ spanning residues 371-400 includes another 23 negatively charged residues, even though it has a shorter tail compared to that of cCSQ from other species (Fig. 7). As shown in the figure 3, the Ca^{2+} binding capacity of the human wild-type cCSQ is slightly lower than that of the canine cCSQ, which is somewhat expected considering the overall net charge of the two proteins. The net charges of the human and canine cCSQ are –64 and –55, respectively based on counting the numbers of arginine, lysine, histidine, aspartate and glutamate residues. Seven out of the nine differences between the two proteins are located in the C-terminal disordered tail. Therefore, except for the remaining two residues, all the charged amino acids in the three thioredoxin domains are conserved between canine and human cCSQ. The two remaining residues Ala88 and Asn228 in the human domains I and II, respectively, are both Asp in canine cCSQ.

As shown in Fig. 6A, the presence in the unit cell of a long, linear polymer of this negatively charged human cCSQ is consistent with the major packing interaction observed in the canine cCSQ crystal and other ultrastructural studies(19,33,34,36). One of the packing interfaces observed in the linear polymer of cCSQ, the front-to-front interface, involves “arm exchange or domain swapping” between the extended amino terminal ends of the two adjacent molecules. The second type of interface, the back-to-back interface, involves bringing together the C-terminals of two symmetry-related molecules. Previously, it was

shown that truncation mutants of the negatively charged C-terminal tail in canine cCSQ remain in the dimer state, probably as front-to-front dimers, without showing any further Ca^{2+}-dependent polymerization(28). In this respect, the recently discovered CPVT-causing truncation mutant, G122+5X(17), may very well be completely non-functional. In addition, the N-terminal extended arm, which contains critical residues for dimerization, is completely conserved between canine and human cCSQ confirming the importance of the N-terminal arm exchange for Ca^{2+}-dependent dynamic polymerization(28). Previously, we also showed that deletion of these critical N-terminal residues leads to a high molecular weight aggregate due to random interactions among CSQ molecules(28). In addition, sequence conservation across both cCSQ and sCSQ molecules also indicates that the residues involved in these back-to-back and front-to-front interfaces are the most highly conserved residues in the entire sequence. This situation is reminiscent of the higher conservation of active-site residues of other proteins, and thus strongly supports our hypothesis that these dimer interfaces are the functional contacts involved in the coupled CSQ polymerization and low affinity Ca^{2+} binding. Any disruption or interference of this critical intermolecular interaction by either mutation or small molecule binding could disrupt the functional integrity of the CSQ molecules(19,46,47).

The CPVT-related mutants result in the observed decrease Ca^{2+} buffering capacity and alteration of the Ca^{2+} release function of the SR in rat myocytes (5,17,48). Currently the exact biochemical impact of the CPVT-related nonsense mutations on cCSQ protein and the mechanism by which these pathophysiological symptoms are being produced, are not clear, even though the biochemical consequence of the truncation, G122+5X, seems obvious as mentioned above. In general, our CD spectra of the CPVT-related mutants (Fig. 1) suggest

that wild type and mutants have similar secondary structures. However, the far UV CD depends mainly on overall secondary structure, thus it is still conceivable that there might be some important structural differences among these mutations as indicated by the difference in fluorescence emission spectra (Fig. 2A). Availability of the 3-D structure of human cCSQ also helps to provide a detailed interpretation of biochemical and biophysical data for CPVT-related mutants. As shown in Fig. 8, the corresponding residues for three severe CPVT forms R33Q, L167H and D307H, are completely conserved among cCSQs and sCSQs of various species. On the other hand, the corresponding residue for the pathologically null mutation, T66A, shows heterogeneity among different species. In cCSQ of rabbit and canine, the corresponding residue is alanine, thus variation of amino acid observed in T66A mutation is already within the polymorphic distribution among the mammals. However, the corresponding residue for another pathophysiologically null mutation, V76M, is conserved among cCSQs, although not in sCSQs. The 3D-structure of human cCSQ indicates that both residues, Thr66 and Val76, reside in the same helix, α3, in domain II. The side chain of the Thr66 does not show any significant interaction with other residues, thus the T66A mutation would not produce any significant structural and biochemical perturbation. The side chain of Val76 is located at the part of α-helix that has an amphiphilic nature. Together with neighboring hydrophobic residues, Leu72 Leu75 and Leu77, and their 2-fold related symmetry equivalent residues, Val 76 establishes a hydrophobic interaction in the front-to-front interface. Therefore the V76M mutation could slightly affect both local conformation of the monomer and its polymeric behavior, as indicated by its altered K^+-dependent fluorescence emission spectra and Ca^{2+}-dependent monomer-dimer transition. Noticeably V76M has a significantly higher proportion of dimers even in the absence of Ca^{2+} ions.

Obviously it shows slightly reduced Ca^{2+}-binding capacity, even though its affinity to junctin seems unaltered.

The CPVT-related mutation, R33Q, produces a more severe reduction in Ca^{2+}-binding capacity than V76M. The conserved residue Arg33 is located between the end of the extended arm and the first β-strand of domain I. Its guanidium group plays a critical role in determining the direction and stability of the N-terminal arm through salt-bridge formation with the side chains of the neighboring acidic residues, Asp29 and Glu85. R33Q mutant shows a similar level of reduction in fluorescence emission as that of V76M (Fig. 2B), in spite of its reduced responsiveness to the increase of K^+ ion. It also follows a similar Ca^{2+}-binding curve in the range below 1mM Ca^{2+} probably reflecting normal Ca^{2+}-binding as a monomer, but defective binding as a dimer or polymer. Previously we showed that in the Ca^{2+} concentration range of 0-1mM, canine cCSQ undergoes a monomer-dimer transition, and at 3mM $CaCl_2$, there is already a detectable amount of tetrameric cCSQ (28). Therefore, considering the location of the mutation and its behaviors, the R33Q mutant loses ability to properly align its extended arm for domain swapping and dimer interaction.

Another CPVT-related residue, Leu167, resides in β3', the third β-strand of the domain II. Its hydrophobic side chain forms the central hydrophobic core of domain II with other surrounding hydrophobic residues, such as Phe182, Phe195, Phe216, Ile227, Leu237 and Phe240. Therefore, the substitution of its original hydrophobic leucine by histidine can result in a serious perturbation of the core as indicated by the biggest change of its CD pattern among the five mutant HcCSQs (Fig. 1). Even though its fluorescence emission level is comparable to those of V76M and R33Q, L167H has a greatly reduced response to both K^+ and Ca^{2+}, displaying characteristics of a heterogeneous polymer state. Overall it shows

the worst Ca^{2+}-binding capacity among the three CPVT-related mutations (Fig. 3). L167H mutant also shows the most reduced Ca^{2+} binding between 0 to 1 mM Ca^{2+} concentration, reflecting both a seriously defective monomer and a consequent failure to form the proper dimer.

Residue 307 is located at the short exposed loop that connects the β2'' and α13 of domain III. Its two neighboring aspartic acids, Asp309 and Asp310, loop back due to residue Pro308 forming a highly negative charged region together with Asp307 itself. In addition, the side chain of Arg251, which has Arg253 and Lys276 as its neighbors, forms a salt-bridge with the side chain of Asp307. Therefore, the D307H mutant can seriously alter the local structure and charge distribution without seriously affecting the content of its local secondary structure. Through molecular modeling, the D307H mutant was predicted previously to have a highly altered protein conformation due to its conversion of a negatively charged aspartic acid into a positively charged histidine, in a highly negatively charged domain (15,45). Most of the residues in the local region around D307 are highly conserved among all the known CSQ sequences (Fig. 7) indicating that it might generate the same effect in all species. All the tryptophan residues are located in domain III, thus local conformational change due to D307H mutation induces the fluorescence quenching effect as shown in a drastic reduction of the fluorescence emission in Fig. 2B. Despite conformational change of the tryptophan residues, its Ca^{2+}-induced monomer-dimer transition pattern and Ca^{2+}-binding capacity as a monomer are closest to those of wild-type among three CPVT-causing mutants.

Previous results for R33Q and L167H indicated that their Ca^{2+}-binding capacities were similar to wild-type cCSQ (5,17). The discrepancy between that study and this might originate from the experimental nature of the Ca^{2+} overlay. Blotting the CSQ molecules onto

nitrocellulose membrane probably does not provide a molecular environment for CSQ to polymerize in a cation-dependent manner due to its immobilization.

Concluding Remarks--The propensity of Ca^{2+}-bound CSQ to form a linear polymer has been closely connected to the unique high capacity and low affinity Ca^{2+}-binding capability of CSQ(28,29). We have proposed that the negative charges on the surface of the dynamic CSQ polymer located near the release channel can act as a Ca^{2+} wire, accelerating Ca^{2+} release by reducing its dimensionality of diffusion (19,36,49). Therefore the change of the polymerization pattern and/or loss of Ca^{2+}-dependency through any mutation or small molecules can reduce both the Ca^{2+}-binding capacity and the conducting (or diffusion) speed. In addition, loss of the ability to interact with junctin and triadin or RyR2 can also result in the loss of localization near the channel preventing Ca^{2+} conduction by CSQ(45). As shown in this article, all three CPVT-related mutant CSQs show significantly altered polymer behavior and reduced Ca^{2+}-binding capacity. Some nonsense mutations produce defective monomer-dimer transitions and other mutants produce a defective monomer or both. These behaviors are all interconnected, however, and are likely to exert deleterious effects by eventually disrupting Ca^{2+}-binding capacity. Putting all the data together, we propose that both the R33Q and D307H mutations result in a monomer that is unable to form a properly oriented dimer even though their monomers have both secondary structure and Ca^{2+}-binding capacity somewhat close to the level of wild-type. These two mutants cannot develop, therefore, into the hypothetical linear polymer or sequester equivalent numbers of Ca^{2+} ions as wild-type. On the other hand, the L167H mutant has a somewhat disrupted hydrophobic core in domain II, resulting in the largest shift from the CD pattern of wild-type and a wide-range of random high molecular aggregates in addition to the monomer, which does not

respond to increasing concentration of Ca^{2+}. One of the pathologically null mutants, T66A, shows little change in Ca^{2+}-binding capacity and light scattering pattern. However, the other null mutant, V76M, does not show a typical Ca^{2+}-dependent response and slightly reduced binding capacity, suggesting that it could potentially generate a pathological problem under certain conditions.

FOOTNOTES

*Original research described in this article was supported by grants to CHK from the National Science Foundation (NSF), the American Heart Association (AHA) and the Murdock Charitable Trust. The authors wish to thank C. Brown, T. Topping, L. Gloss, and G. Munske for helpful discussion and suggestion.

Referencres

1. **Scheinman, M., and Lam, J.** (2006) *Annu Rev Med.* **57**, 473-484.

2. **Postma, A., Denjoy, I., Hoorntje, T., Lupoglazoff, J., Da Costa, A., Sebillon, P., Mannens, M., Wilde, A., and Guicheney, P.** (2002) *Circ Res.* **91**, 21-26

3. **Viskin, S., and Belhassen, B.** (1998) *Prog Cardiovasc Dis.* **41**, 17-34.

4. **Lahat, H., Pras, E., and Eldar, M.** (2004) *Ann Med.* **36 Suppl 1**, 87-91.

5. **Terentyev, D., Nori, A., Santoro, M., Viatchenko-Karpinski, S., Kubalova, Z., Gyorke, I., Terentyeva, R., Vedamoorthyrao, S., Blom, N., Valle, G., Napolitano, C., Williams, S., Volpe, P., Priori, S., and Gyorke, S.** (2006) *Circ Res.* **98**, 1151-1158.

6. **Kontula, K., Laitinen, P., Lehtonen, A., Toivonen, L., Viitasalo, M., and Swan, H.** (2005) *Cardiovasc Res.*, [Epub ahead of print]

7. **Bauce, A., Rampazzo, A., Basso, C., Bagattin, A., Daliento, L., and Tiso, N. e. a.** (2002) *J Am Coll Cardiol* **40**, 341-349

8. **Rubart, M., Lopshire, J., Fineberg, N., and Zipes, D.** (2000) *Cardiovasc Electrophysiol.* **11**, 652-664.

9. **Miyata, A., Dowell, J., Zipes, D., and Rubart, M.** (2002) *Am J Physiol Heart Circ Physiol.* **283**, H506-517.

10. **Laitinen, P., Brown, K., Piippo, K., Swan, H., Devaney, J., Brahmbhatt, B., Donarum, E., Marino, M., Tiso, N., Viitasalo, M., Toivonen, L., Stephan, D., and** Kontula, K. (2001) *Circulation.* 103, 485-490

11. **Priori, S., Napolitano, C., Tiso, N., Memmi M, Vignati G, Bloise R, Sorrentino VV, and GA., D.** (2001) *Circulation* **103**, 196–200.

12. **Swan, H., Piippo, K., Viitasalo, M., Heikkila, P., Paavonen, T., Kainulainen, K., Kere, J., Keto, P., Kontula, K., and Toivonen, L.** (1999) *J Am Coll Cardiol.* **34**, 2035-2042.

13. **Thomas, N., George, C., and Lai, F.** (2006) *Biochem Soc Trans.* **34**, 913-918

14. **Lahat, H., Pras, E., Olender, T., Avidan, N., Ben-Asher, E., Man, O., Levy-Nissenbaum, E., Khoury, A., Lorber, A., Goldman, B., Lancet, D., and Eldar, M.** (2001) *Am J Hum Genet.* **69**, 1378-1384.

15. **Eldar, M., Pras, E., and Lahat, H.** (2003) *Trends Cardiovasc Med.*, 148-151.

16. **Laitinen, P., Swan, H., and Kontula, K.** (2003) *Eur J Hum Genet.* **11**, 888-891.

17. **di Barletta, M., Viatchenko-Karpinski, S., Nori, A., Memmi, M., Terentyev, D., Turcato, F., Valle, G., Rizzi, N., Napolitano, C., Gyorke, S., Volpe, P., and Priori, S.** (2006) *Circulation* **114**, 1012-1019.

18. **MacLennan, D., and Wong, P.** (1971) *Proc Natl Acad Sci U S A* **68**, 1231-1235

19. **Park, H., Park, I.-Y., Kim, E., Youn, B., Fields, K., Dunker, A., and Kang, C.** (2004) *J Biol Chem* **279**, 18026-18033

20. **Gyorke, S., Gyorke, I., Terentyev, D., Viatchenko-Karpinski, S., and Williams, S.** (2004) *Biol Res.* **37**, 603-607.

21. **Terentyev, D., Viatchenko-Karpinski, S., Gyorke, I., Volpe, P., Williams, S., and Gyorke, S.** (2003) *Proc Natl Acad Sci U S A.* **100**, 11759-11764

22. **Tanaka, M., Ozawa, T., Maurer, A., Cortese, J., and Fleischer, S.** (1986) *Arch Biochem Biophys* **251**, 369-378.

23. **Ikemoto, N., Bhatnagar, G., Nagy, B., and Gergely, J.** (1972) *J Biol Chem.* **247**, 7835-7837

24. **MacLennan, D.** (1974) *J Biol Chem.* **249**, 980-984.

25. **Aaron, B., Oikawa, K., Reithmeier, R., and Sykes, B.** (1984) *J Biol Chem* **259**, 11876-11881.

26. **Slupsky, J., Ohnishi, M., Carpenter, M., and Reithmeier, R.** (1987) *Biochemistry.* **26**, 6539-6544.

27. **Ikemoto, N., Antoniu, B., Kang, J., Meszaros, L., and Ronjat, M.** (1991) *Biochemistry* **30**, 5230-5237.

28. **Park, H., Wu, A., Dunker, A., and Kang, C.** (2003) *J Biol Chem* **278**

29. **Launikonis, B., Zhou, J., Royer, L., Shannon, T., Brum, G., and Rios, E.** (2006) *Proc Natl Acad Sci U S A.* **103**, 2982-2987

30. **Maurer, A., Tanaka, M., Ozawa, T., and Fleischer, S.** (1985) *Proc Natl Acad Sci U S A* **82**, 4036-4040

31. **Williams, R., and Beeler, T.** (1986) *J Biol Chem.* **261**, 12408-12413

32. **Hayakawa, K., Swenson L, Baksh S, Wei Y, Michalak M, and ZS., D.** (1994) *J Mol Biol.* **235**, 357-360

33. **Franzini-Armstrong, C., Kenney, L., and Varriano-Marston, E.** (1987) *J Cell Biol* **105**, 49-56.

34. **Saito, A., Seiler, S., Chu, A., and Fleischer, S.** (1984) *J Cell Biol* **99**, 875-885

35. **Maguire, P., Briggs FN, Lennon NJ, and Ohlendieck, K.** (1997) *Biochem Biophys Res Commun.* **240**, 721-727.

36. **Wang, S., Trumble, W., Liao, H., Wesson, C., Dunker, A., and Kang, C.** (1998) *Nat Struct Biol* **5**, 476-483

37. **Caswell, A., Brandt, N., Brunschwig, J., and Purkerson, S.** (1991) *Biochemistry* **30**, 7507-7513

38. **Knudson, C., Stang KK, Jorgensen AO, and Campbell, K.** (1993) *J Biol Chem.* **268**, 12637-12645.

39. **Guo, W., Jorgensen, A., Jones, L., and Campbell, K.** (1996) *J Biol Chem* **271**, 458-465

40. **Jones, L., Zhang, L., Sanborn, K., Jorgensen, A., and Kelley, J.** (1995) *J Biol Chem.* **270**, 30787-30796.

41. **Zhang, L., Kelley, J., Schmeisser, G., Kobayashi, Y., and Jones, L.** (1997) *J Biol Chem* **272**, 23389-23397

42. **Kirchhof, P., Klimas, J., and Fabritz, L.** (2004) *Heart Rhythm* **1:S64 (Abstr.)**

43. **Mitchell, R., Simmerman, H., and Jones, L.** (1988) *J Biol Chem.* **263**, 1376-1381

44. **Kobayashi, Y., Alseikhan, B., and Jones, L.** (2000) *J Biol Chem* **275**, 17639-17646

45. **Houle, T., Ram, M., and Cala, S.** (2004) *Cardiovasc Res.* **64**, 227-233.

46. **Park, I., Kim, E., Park, H., Fields, K., Dunker, K., and Kang, C.** (2005) *J. Mol. Pharmacology* **67**, 95-105

47. **Kim, E., Tam, M., Siems, WF,, and Kang, C.** (2005) *Mol Pharmacol.* **68**, 1708-1715.

48. **Viatchenko-Karpinski, S., Terentyev, D., Gyorke, I., Terentyeva, R., Volpe, P., Priori, S., Napolitano, C., Nori, A., Williams, S., and Gyorke, S.** (2004) *Circ Res.* **94**, 471-477

49. **MacLennan, D., and Reithmeier, R.** (1998) *Nat Struct Biol* **5**, 409-411

Figure legends

Fig. 1. Far UV CD spectra of wild type and mutants HcCSQs. 0.35mg/ml of each protein was buffered in 10 mM MOPS (pH 7.2) with 300 mM KCl. CD spectra were collected from 200 to 260nm wavelength with 1nm bandwidth. (Inset) WT and mutant HcCSQ samples used for CD measurement were shown in 12% SDS-PAGE stained with coomassie blue. Wild type and mutant HcCSQ proteins (R33Q, T66A, V76M, L167H, D307H) were purified and used for CD measurement as described in Experimental Procedures.

Fig. 2. A) KCl dependent intrinsic fluorescence changes of wild type and mutant HcCSQs at 330nm: K+ induced fluorescence of 20μg of wild type and mutants were observed ranging from 310 to 400nm. B) To better visualize the fluorescence changes upon addition of KCl, fluorescence at 330nm under 0mM KCl conditions was normalized to a value of 1 and the percentage changes in fluorescence observed at 330nm for each KCl concentration [mM] were plotted.

Fig. 3. Ca^{2+}-binding capacities of HcCSQs. The number of Ca^{2+} bound to wild type and mutants was determined through equilibrium dialysis and atomic absorption spectroscopy. Fractional occupancy (y = [bound Ca^{2+}] / [total protein]) was plotted against unbound Ca^{2+} concentration [mM]. The lines were drawn for the ease of view.

Fig. 4. Linear gradient SDS-PAGE (10-14%) of DTSSP Cross-linked Wild-type and Mutant cCSQs. Each protein sample was pre-incubated with 150mM KCl (Left lanes for each protein) and 150mM KCl, 2mM $CaCl_2$ (Right lanes for each protein). After pre-incubation, all samples were incubated with DTSSP (final 0.1mM). Far left side lane is the molecular weights marker.

Fig. 5. Multi-angle laser light scattering elution profiles of wild-type and mutant HcCSQs with and without Ca^{2+} ions. Elusion profiles are shown as molecular weight (D_a) versus elution volume (ml). The red line in each graph indicates the elution profile of each calsequestrin in the presence of 1mM $CaCl_2$ and the green line represents the elution profile in the absence of Ca^{2+} ions. The red and green horizontal bars indicate the calculated molecular mass of the corresponding peaks. The different colors indicate different polymerization states of the calsequestrins.

Fig. 6. A) Diagram illustrating the unit cell packing interaction of the sixteen calsequestrin molecules in the crystal lattice. Human cCSQ was crystallized in the space group I422 with unit cell dimensions of a = b = 150.65Å, c = 227.47Å with one molecule per asymmetric unit. The major lattice packing interaction observed in this calsequestrin crystal is along the long linear polymer.

B) Ribbon diagram of human cardiac calsequestrin showing the distribution of structural elements. The N- and C- termini are labeled. The amino acids corresponding to the two null mutations (T66A and V76M) and three CPVT-related mutations (R33Q, L167H, D307H) are indicated by the pink stick model and the corresponding van der Waals surface.

The topology of an individual domain is identical with that of *E.coli* thioredoxin. This figure was prepared using PyMOL v0.99.

Fig. 7. Amino acid sequence comparison of cardiac calsequestrin from human, canine, rabbit, chicken and Xenopus and human skeletal calsequestrin. Five mutational sites (R33, T66, V76, L167 and D307) are highlighted in green and the mutation was named according to the amino acid number in the unprocessed protein in calsequestrin. The signal peptides are indicated with the black dashed box. The secondary structural elements are indicated with colored arrows on top of the corresponding sequences and each domain (I, II and III) is marked with green lines.

Fig.1

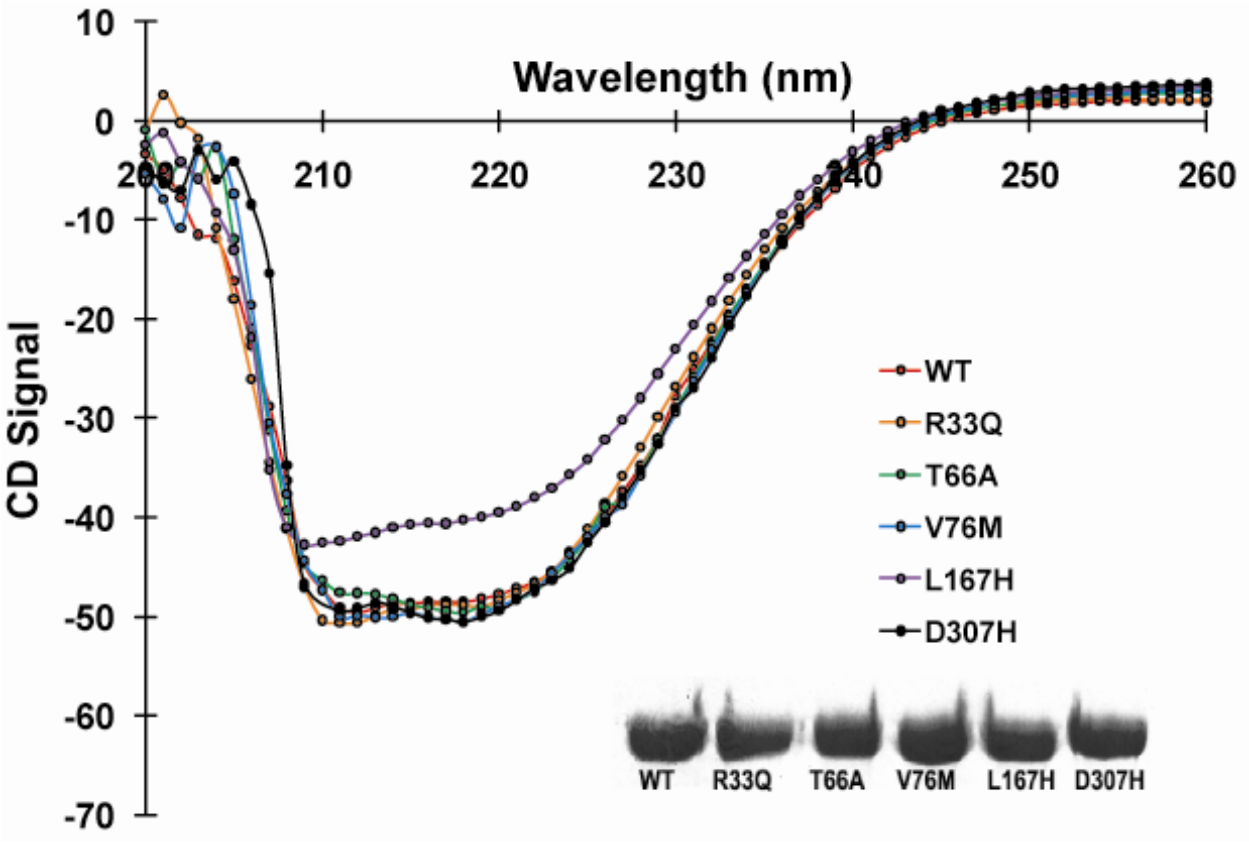
Wavelength (nm)
CD Signal
10
0
-10
-20
-30
-40
-50
-60
-70
200
210
220
230
240
250
260
WT
R33Q
T66A
V76M
L167H
D307H
WT
R33Q
T66A
V76M
L167H
D307H

Fig. 2

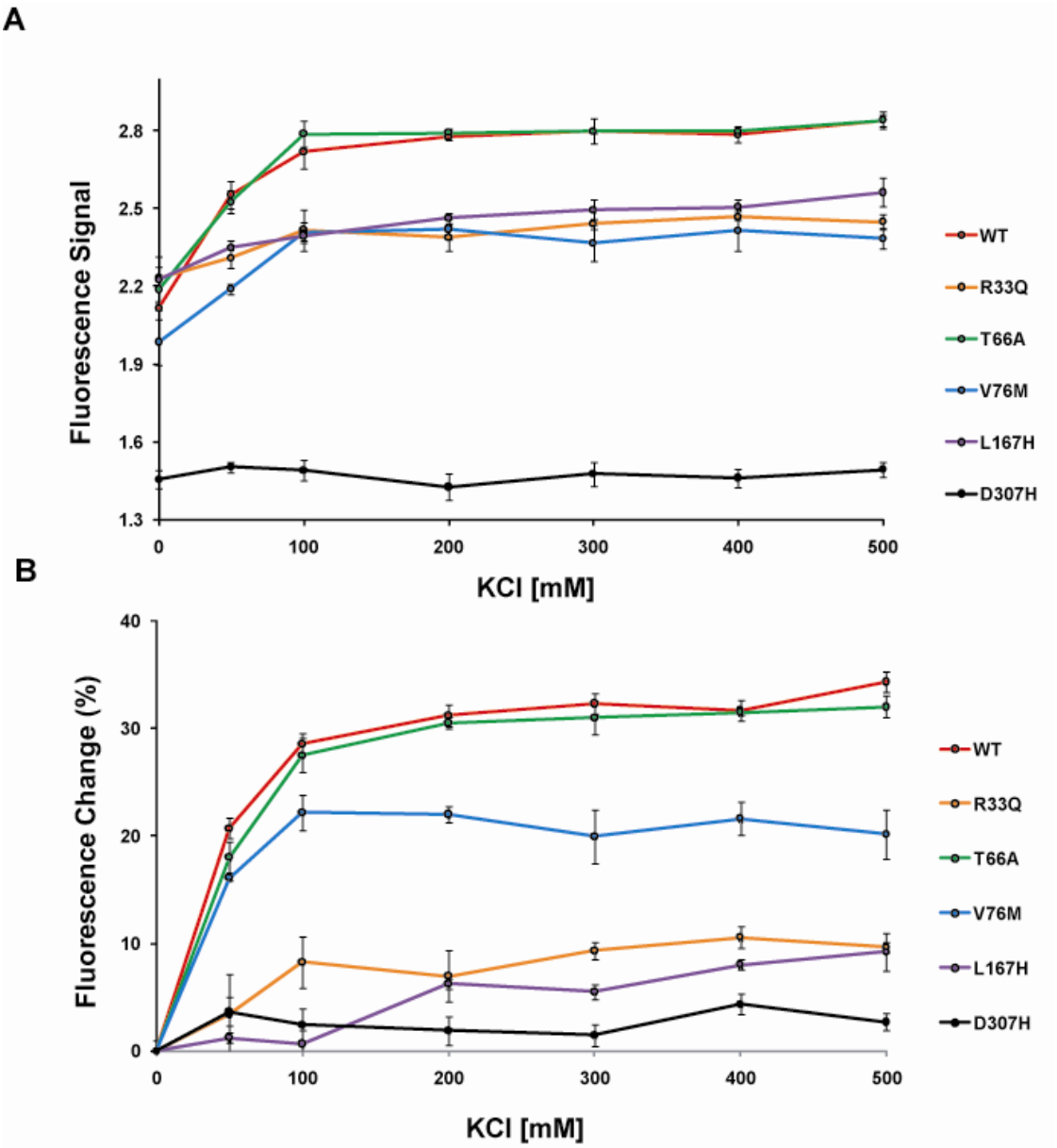
A
Fluorescence Signal
2.8
2.5
2.2
1.9
1.6
1.3
0
100
200
300
400
500
KCl [mM]
WT
R33Q
T66A
V76M
L167H
D307H
B
Fluorescence Change (%)
40
30
20
10
0
0
100
200
300
400
500
KCl [mM]
WT
R33Q
T66A
V76M
L167H
D307H

Fig. 3

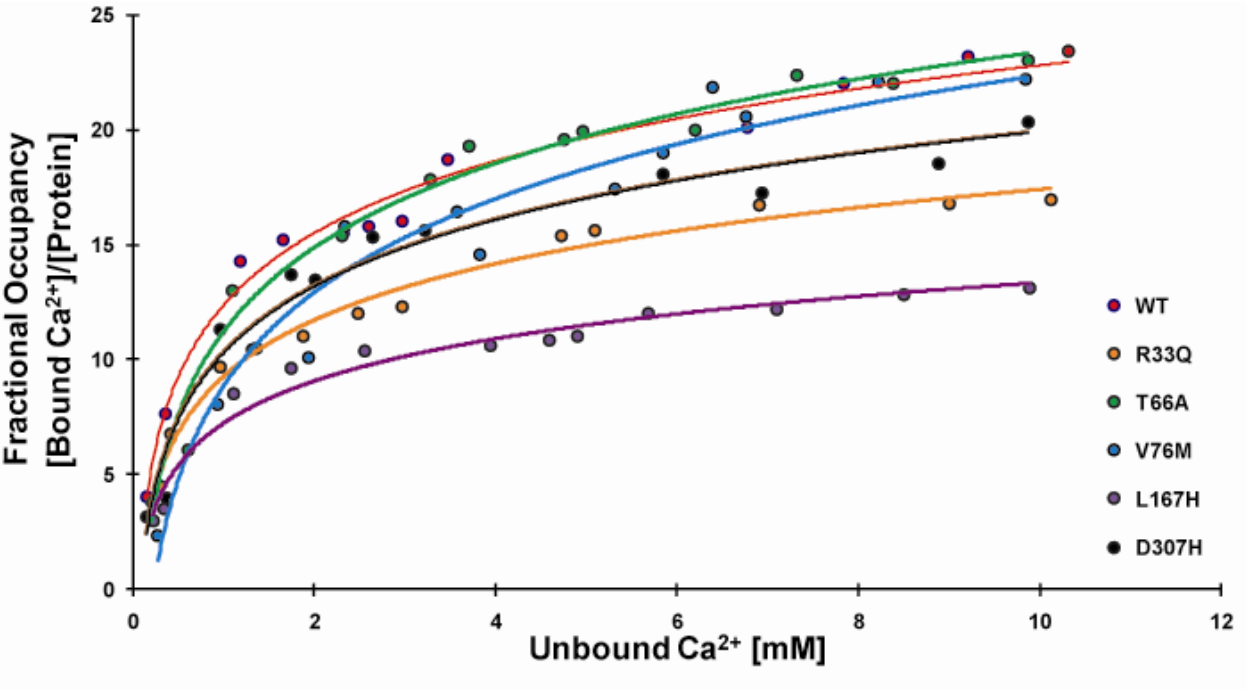
Fractional Occupancy
[Bound Ca2+]/[Protein]
Unbound Ca2+ [mM]
0
5
10
15
20
25
0
2
4
6
8
10
12
WT
R33Q
T66A
V76M
L167H
D307H

Fig.4

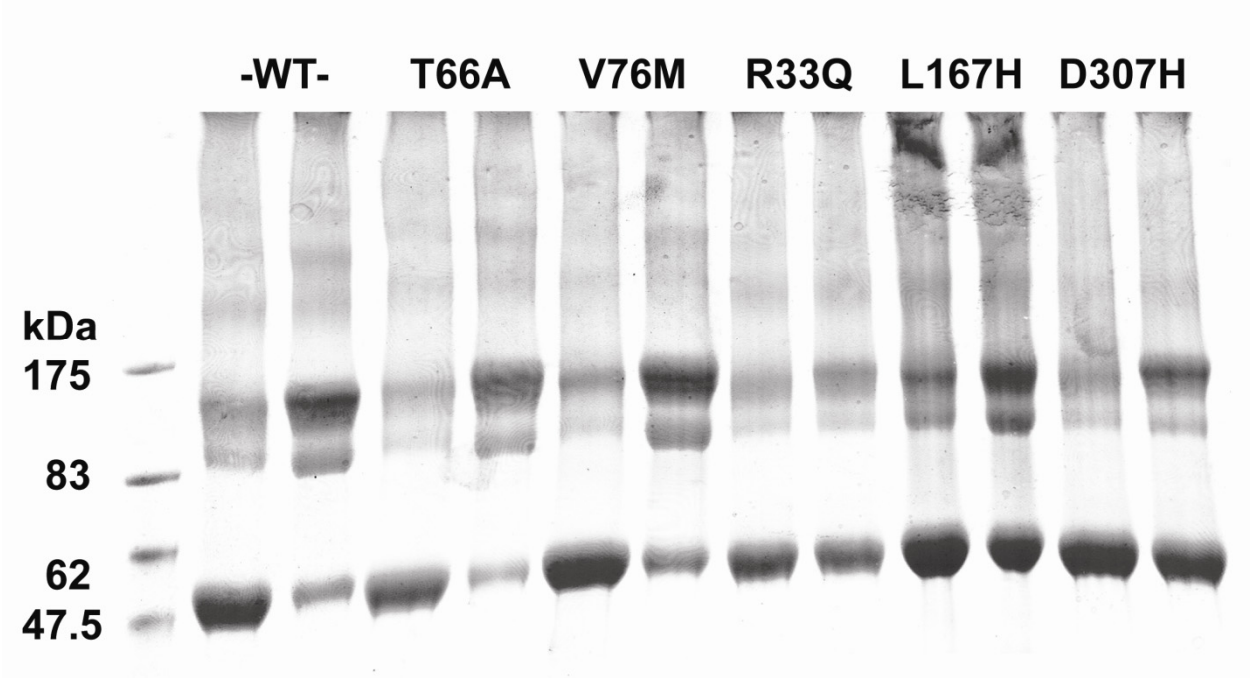

Fig.5

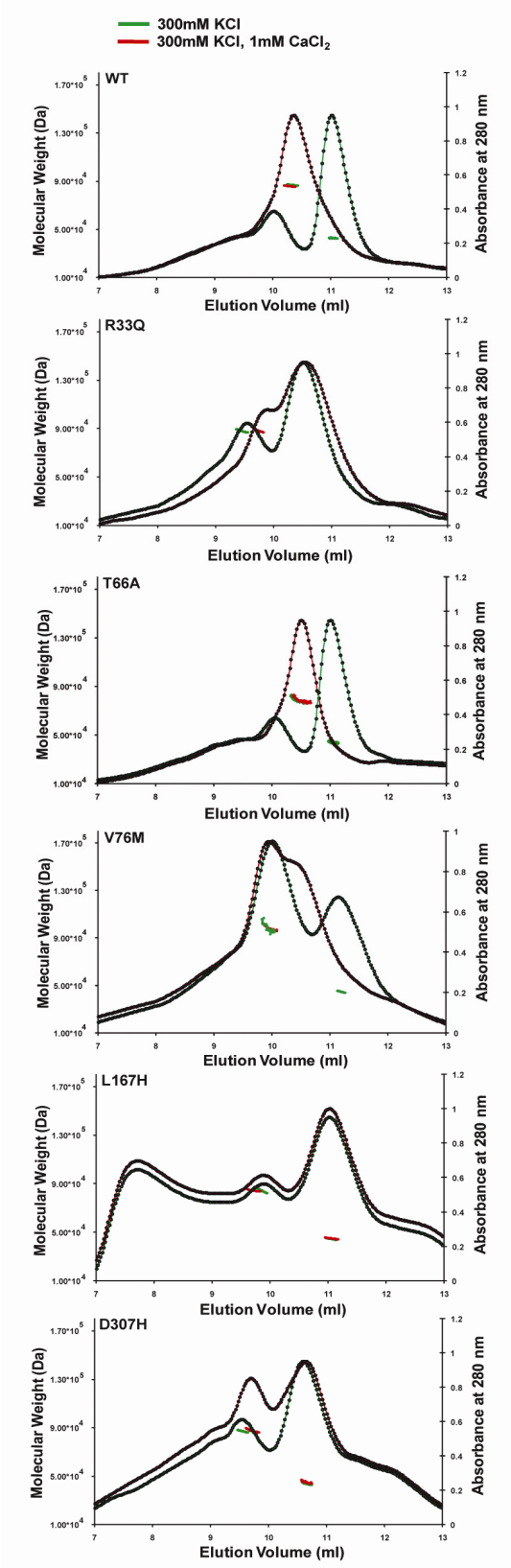
300mM KCl
300mM KCl, 1mM CaCl2
WT
R33Q
T66A
V76M
L167H
D307H
Molecular Weight (Da)
Absorbance at 280 nm
Elution Volume (ml)

Fig. 6A

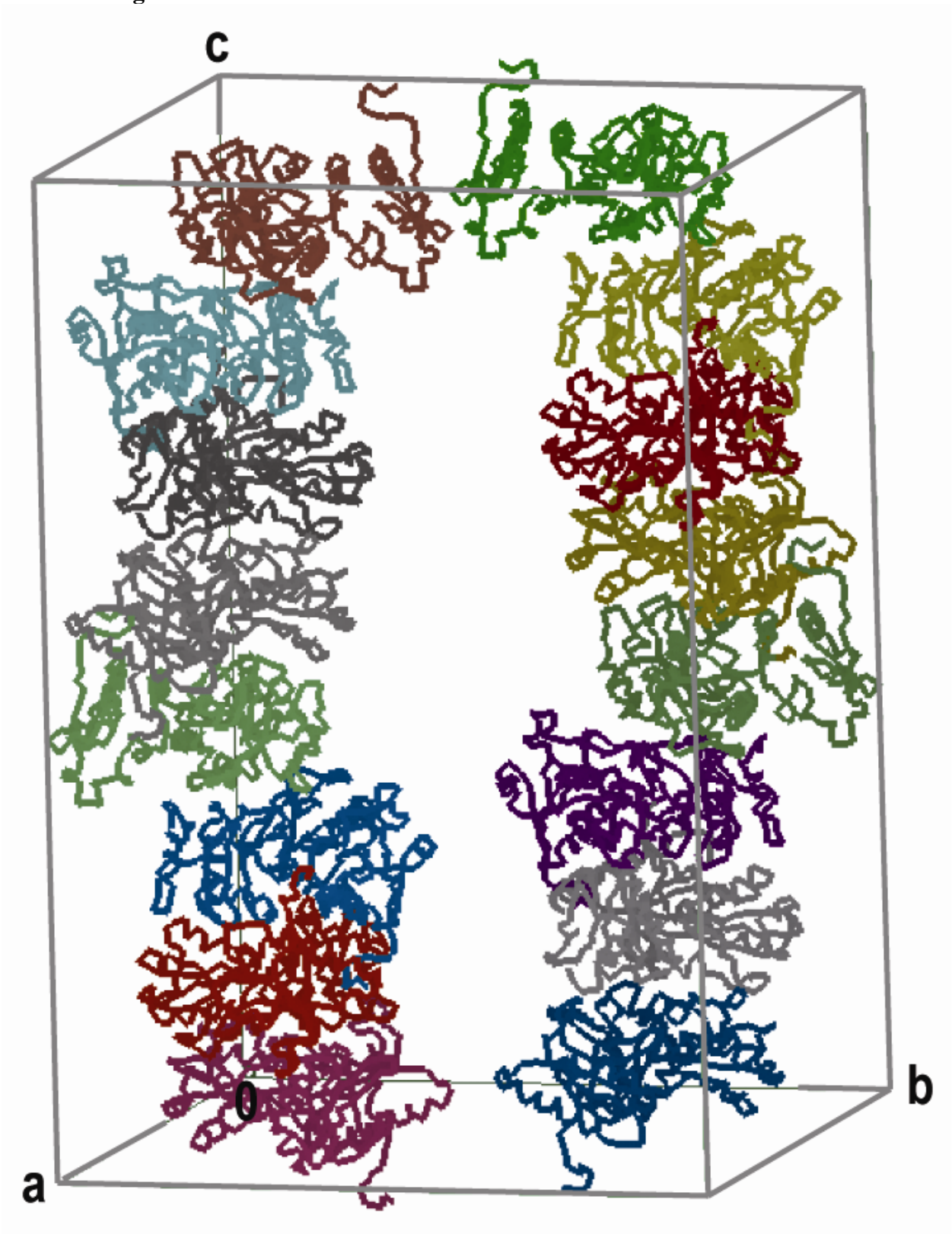

Fig.6B

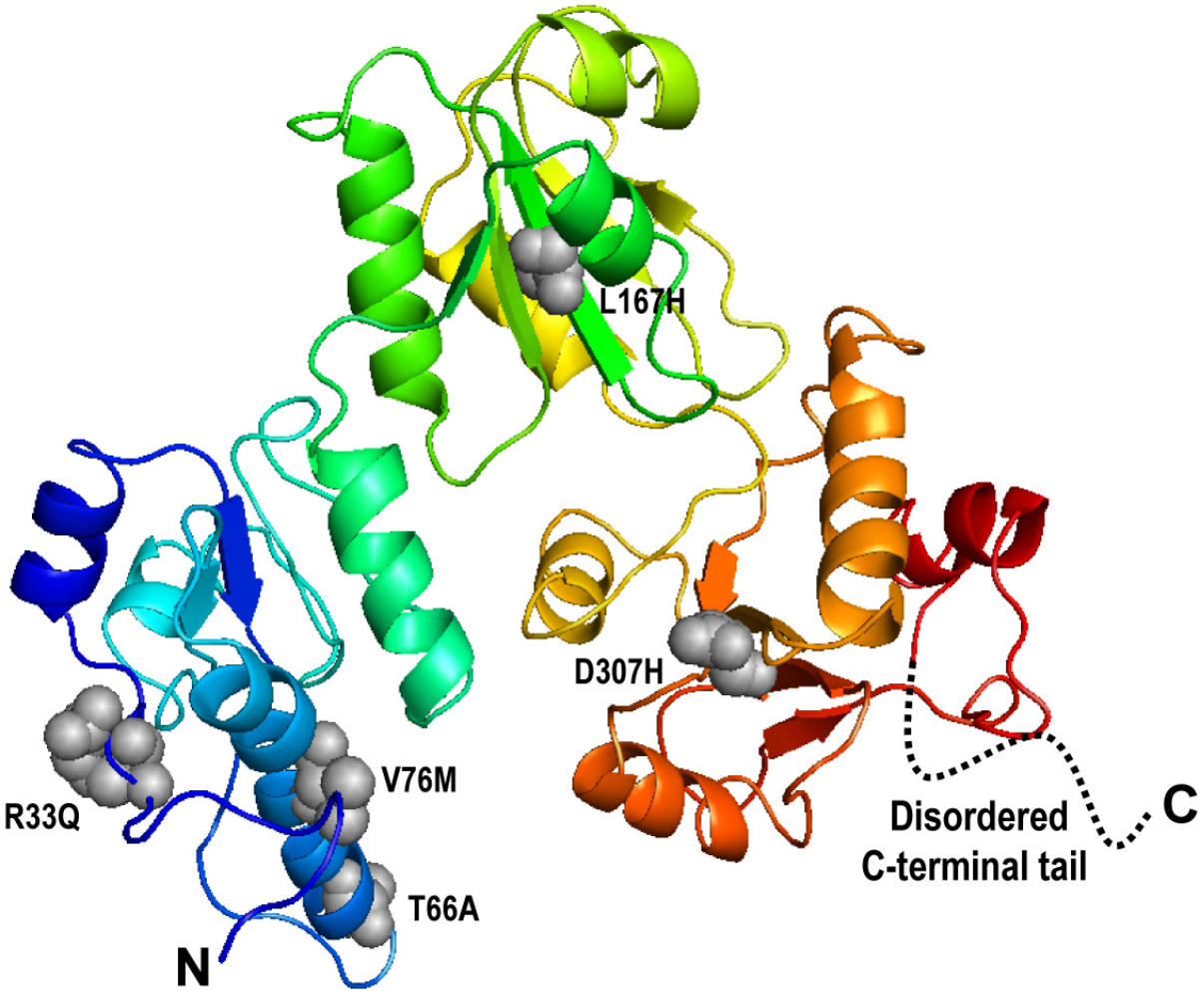

Fig. 7

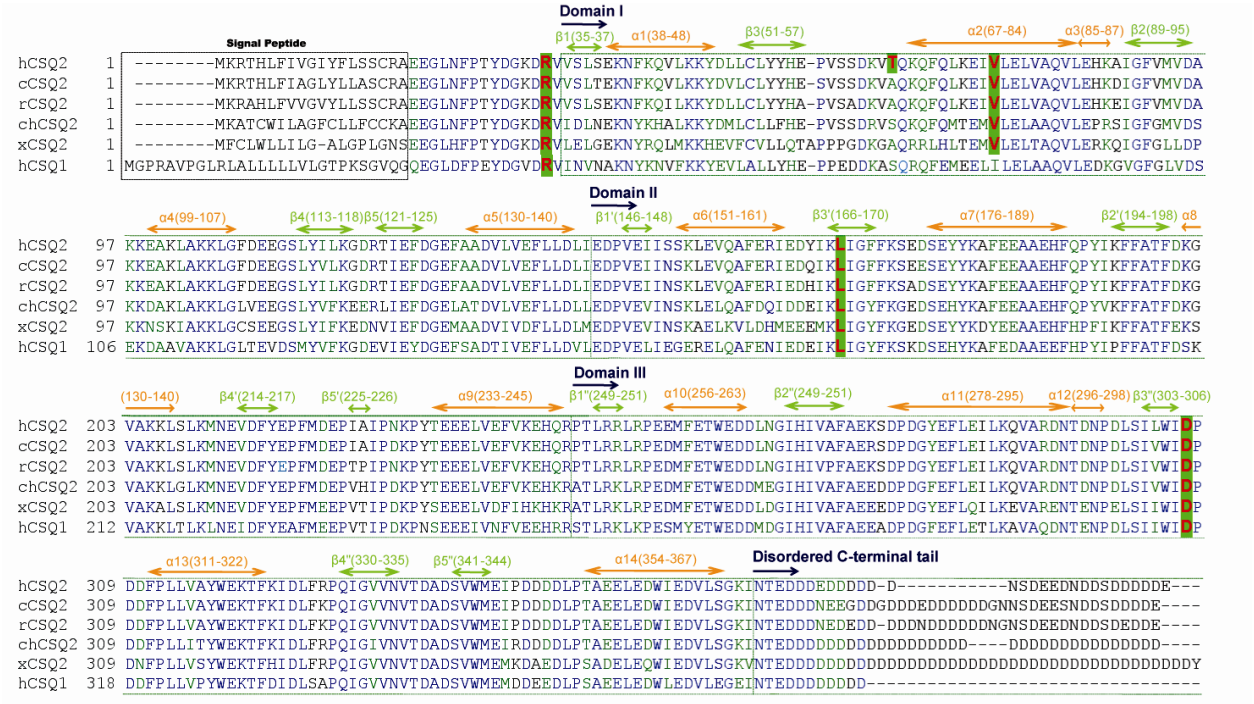
Domain I
Signal Peptide
β1(35-37)
α1(38-48)
β3(51-57)
α2(67-84)
α3(85-87)
β2(89-95)
hCSQ2 1 --------MKRTHLFIVGIYFLSSCRAEEGLNFPTYDGKDRVVSLSEKNFKQVLKKYDLLCLYYHE-PVSSDKVTQKQFQLKEIVLELVAQVLEHKAIGFVMVDA
cCSQ2 1 --------MKRTHLFIAGLYLLASCRAEEGLNFPTYDGKDRVVSLTEKNFKQVLKKYDVLCLYYHE-SVSSDKVAQKQFQLKEIVLELVAQVLEHKDIGFVMVDA
rCSQ2 1 --------MKRAHLFVVGVYLLSSCRAEEGLNFPTYDGKDRVVSLSEKNFKQILKKYDLLCLYYHA-PVSADKVAQKQFQLKEIVLELVAQVLEHKEIGFVMVDA
chCSQ2 1 --------MKATCWILAGFCLLFCCKAEEGLNFPTYDGKDRVIDLNEKNYKHALKKYDMLCLLFHE-PVSSDRVSQKQFQMTEMVLELAAQVLEPRSIGFGMVDS
xCSQ2 1 --------MFCLWLLILG-ALGPLGNSEEGLHFPTYDGKDRVLELGEKNYRQLMKKHEVFCVLLQTAPPPGDKGAQRRLHLTEMVLELTAQVLERKQIGFGLLDP
hCSQ1 1 MGPRAVPGLRLALLLLLVLGTPKSGVQGQEGLDFPEYDGVDRVINVNAKNYKNVFKKYEVLALLYHE-PPEDDKASQRQFEMEELILELAAQVLEDKGVGFGLVDS
Domain II
α4(99-107)
β4(113-118)β5(121-125)
α5(130-140)
β1'(146-148)
α6(151-161)
β3'(166-170)
α7(176-189)
β2'(194-198)
α8
hCSQ2 97 KKEAKLAKKLGFDEEGSLYILKGDRTIEFDGEFAADVLVEFLLDLIEDPVEIISSKLEVQAFERIEDYIKLIGFFKSEDSEYYKAFEEAAEHFQPYIKFFATFDKG
cCSQ2 97 KKEAKLAKKLGFDEEGSLYVLKGDRTIEFDGEFAADVLVEFLLDLIEDPVEIINSKLEVQAFERIEDQIKLIGFFKSEESEYYKAFEEAAEHFQPYIKFFATFDKG
rCSQ2 97 KKEAKLAKKLGFDEEGSLYILKGDRTIEFDGEFAADVLVEFLLDLIEDPVEIINSKLEVQAFERIEDHIKLIGFFKSADSEYYKAFEEAAEHFQPYIKFFATFDKG
chCSQ2 97 KKDAKLAKKLGLVEEGSLYVFKEERLIEFDGELATDVLVEFLLDLIEDPVEVINSKLELQAFDQIDDEIKLIGYFKGEDSEHYKAFEEAAEHFQPYVKFFATFDKG
xCSQ2 97 KKNSKIAKKLGCSEEGSLYIFKEDNVIEFDGEMAADVIVDFLLDLMEDPVEVINSKAELKVLDHMEEEMKLIGYFKGEDSEYYKDYEEAAEHFHPFIKFFATFEKS
hCSQ1 106 EKDAAVAKKLGLTEVDSMYVFKGDEVIEYDGEFSADTIVEFLLDVLEDPVELIEGERELQAFENIEDEIKLIGYFKSKDSEHYKAFEDAAEEFHPYIPFFATFDSK
Domain III
(130-140)
β4'(214-217)
β5'(225-226)
α9(233-245)
β1''(249-251)
α10(256-263)
β2''(249-251)
α11(278-295)
α12(296-298)
β3''(303-306)
hCSQ2 203 VAKKLSLKMNEVDFYEPFMDEPIAIPNKPYTEEELVEFVKEHQRPTLRRLRPEEMFETWEDDLNGIHIVAFAEKSDPDGYEFLEILKQVARDNTDNPDLSILWIDP
cCSQ2 203 VAKKLSLKMNEVDFYEPFMDEPIAIPDKPYTEEELVEFVKEHQRPTLRRLRPEDMFETWEDDLNGIHIVAFAERSDPDGYEFLEILKQVARDNTDNPDLSIVWIDP
rCSQ2 203 VAKKLSLKMNEVDFYEPFMDEPTPIPNKPYTEEELVEFVKEHQRPTLRRLRPEDMFETWEDDLNGIHIVPFAEKSDPDGYEFLEILKQVARDNTDNPDLSIVWIDP
chCSQ2 203 VAKKLGLKMNEVDFYEPFMDEPVHIPDKPYTEEELVEFVKEHKRATLRKLRPEDMFETWEDDMEGIHIVAFAEEDDPDGFEFLEILKQVARDNTDNPDLSIVWIDP
xCSQ2 203 VAKALSLKMNEVDFYEPFMEEPVTIPDKPYSEEELVDFIHKHKRATLRKLRPEDMFETWEDDLDGIHIVAFAEEEDPDGYEFLQILKEVARENTENPELSIIWIDP
hCSQ1 212 VAKKLTLKLNEIDFYEAFMEEPVTIPDKPNSEEEIVNFVEEHRRSTLRKLKPESMYETWEDDMDGIHIVAFAEEADPDGFEFLETLKAVAQDNTENPDLSIIWIDP
α13(311-322)
β4''(330-335)
β5''(341-344)
α14(354-367)
Disordered C-terminal tail
hCSQ2 309 DDFPLLVAYWEKTFKIDLFRPQIGVVNVTDADSVWMEIPDDDDLPTAEELEDWIEDVLSGKINTEDDDEDDDDD-D----------NSDEEDNDDSDDDDDE---
cCSQ2 309 DDFPLLVAYWEKTFKIDLFKPQIGVVNVTDADSVWMEIPDDDDLPTAEELEDWIEDVLSGKINTEDDDNEEGDDGDDDEDDDDDDGNNSDEESNDDSDDDDE----
rCSQ2 309 DDFPLLVAYWEKTFKIDLFKPQIGVVNVTDADSVWMEIPDDDDLPTAEELEDWIEDVLSGKINTEDDDNEDEDD-DDDNDDDDDDNGNSDEEDNDDSDEDDE----
chCSQ2 309 DDFPLLITYWEKTFKIDLFRPQIGIVNVTDADSVWMEIRDDDDLPTAEELEDWIEDVLSGKINTEDDDDDDDDDDDDDDDDDD----DDDDDDDDDDDDDD----
xCSQ2 309 DNFPLLVSYWEKTFHIDLFRPQIGVVNVTDADSVWMEMKDAEDLPSADELEQWIEDVLSGKVNTEDDDDDDDDDDDDDDDDDDDDDDDDDDDDDDDDDDDDDY
hCSQ1 318 DDFPLLVPYWEKTFDIDLSAPQIGVVNVTDADSVWMEMDDEEDLPSAEELEDWLEDVLEGEINTEDDDDDDDD-----------------------------

CHAPTER THREE

CRYSTALLIZATION REPORT OF CANINE CARDIAC JUNCTIN

Preface

Junctin is an integral membrane protein that is colocalized with the Ca^{2+} release channel (ryanodine receptor), triadin and calsequestrin at the junctional sarcoplasmic reticulum (SR) membrane in both cardiac and skeletal muscle. Junctin is one of the putative anchoring proteins that appear to stabilize calsequestrin at the luminal side of SR membrane for the normal operation of Ca^{2+} regulation. However, to date, little is known about the biological roles of junctin and how it is able to interact directly with the Ca^{2+} release channel complex.

To better understand the role of junctin, we successfully crystallized the canine cardiac junction. The following chapter reports a preliminary structural study of junctin.

A supplemental section of the crystallographic methods follows the paper to aid reader's understanding.

Crystallization and Preliminary X-Ray Analysis of Canine Cardiac Junctin

EunJung Kim, BuHyun Youn and ChulHee Kang

School of Molecular Biosciences, Washington State University, Pullman, WA 99164-4660

Summary

Junctin is one of the main components of the ryanodine receptor Ca^{2+} release channel complex in the sarcoplasmic reticulum membrane. In addition to junctin, the complex components are the ryanodine receptor, triadin and calsequestrin. Although in the channel complex, junctin appears to sense the changes of Ca^{2+} concentration for the ryanodine receptor channel opening, the exact role of junctin is still uncertain and remained to be determined. Therefore, the atomic resolution structure can help to delineate its function.

The canine cardiac junctin was crystallized by the hanging drop diffusion method with an ammonium sulfate based solution. Preliminary X-ray diffraction studies of the junctin crystal show that it belongs to the tetragonal space group I422. The unit cell dimensions are a=121.3652, b=121.3652, c=136.6409 Å. A complete diffraction data set for junctin was collected to 2.6 Å. To solve the phase problem, various methods such as heavy atom soaking and selenium methionine substitution methods are being applied.

FOOTNOTES AND ABBREVIATIONS

The abbreviations used in this work are:

SR**,** Sarcoplasmic Reticulum

MIR, Multiple Isomorphous Replacement

MAD, Multiple wavelength anomalous dispersion.

Introduction

The sarcoplasmic reticulum (SR) Ca^{2+} release channel complex plays an essential role in muscle contraction and relaxation processES. The complex includes several proteins; the ryanodine receptor, triadin, junctin and calsequetrin, which are colocalized to the Ca^{2+} release site and an important for Ca^{2+} release and re-uptake during muscle movement in the junctional sarcoplasmic reticulum (1; 2) . Calsequestrin is a high capacity, low affinity Ca^{2+} binding protein found in the SR of skeletal and cardiac muscle (3; 4). Calsequestrin acts as a Ca^{2+} buffer inside the SR by lowering free Ca^{2+} concentrations and localizes Ca^{2+} in the vicinity of the Ca^{2+} release site to regulate the amount of Ca^{2+} released through the ryanodine receptor (5; 6; 7). Junctin is the anchoring protein directly to the ryanodine receptor and calsequestrin in the inner face of SR membrane (8). There are three segments in this 26kDa protein and those segments are a short cytoplasmic N-terminal tail region (from 1 to 22 residues), transmembrane region (from 22 to 44), and the rest of the residues among 210 amino acids is long and located in the lumen. The long stretch luminal segment with highly charged residues contains a repeated KEKE motif and this is reported to be associated with direct interaction between itself and the other ryanodine channel complex components to regulate the ryanodine receptor Ca^{2+} release (8; 9). However, the functional role of junctin is still uncertain and remains to be determined.

Therefore, in order to understand and interpret how junctin interacts directly to the ryanodine receptor and calsequestrin for the normal Ca^{2+} regulation, we recently cloned and purified canine cardiac junctin. The first 44 amino acids corresponding to the transmembrane portion of the protein was deleted due to the solubility problem and the potential difficulty in

crystallization. Successfully, we have obtained the crystal of recombinant junctin and the preliminary x-ray diffraction was analyzed. To determine the phase of the reflection data, many approaches are being applied now.

Methods

Expression and purification of recombinant Junctin : After deletion of nucleotides corresponding to 44 amino acids N- terminal transmembrane domain in Junctin, canine cardiac junctin containing SalI and XhoI sites was subcloned into pET24b and overexpressed in the *E.coli* strain, ER2566. Cells were grown in YEP media (Bacto peptone 20g and yeast extract 10g in 1L dH_2O) containing kanamycin 30 µg/ml until the OD_{600} reached 0.8 at 37 °C and then 0.5mM IPTG was added to start induction at 30 °C for 10 hours. For purification of junctin, nickel-nitrilotriacetic acid agarose (Qiagen, Hilden, Germany) was used initially. After harvesting cells, cells were sonicated (5 x 10 s, model 450 Sonifier®, Branson Ultrasonics) in wash buffer (50mM NaH_2PO_4, 300mM NaCl, 20mM imidazole pH8.0), followed by centrifugation at 20,000 x g for 40 minutes. The supernatant was then applied to the pre-equilibriated Ni-NTA column with a wash buffer, followed by protein elution. The elution buffer contains 50mM NaH_2PO_4, 300mM NaCl and 250mM imidazole with final pH 8.0. For further purification, Junctin was applied to poros HS-20 (Amersham Biosciences) column and junctin buffer was changed to buffer A containing 20mM sodium phosphate, pH6.8. Junctin was eluted by a step gradient between buffer A and buffer B (20mM sodium phosphate pH6.8 and 2M NaCl).

Crystallization of Junctin*:* For crystallization, 5mg/ml of purified junctin in 20mM sodium acetate pH 5.5 containing 0.5mM $CaCl_2$ was prepared and crystallization trials were carried out through the hanging drop vapor diffusion method at 4ºC. Junctin crystals were obtained by mixing the above purified junctin (1.5 µl) with an equal volume of reservoir solution containing 2M Ammonium Sulfate and 5% isopropanol. Crystals usually appeared after 30 days and they were in a hexagonal shape.

X-ray data collection: The crystals of junctin belong to the tetragonal space group, *I422* (*a* = 121.3652, *b* = 121.3652, *c* = 136.6409 Å) (Table. 1). The data set for junctin (2.6 Å resolution) was collected from the Berkeley Advanced Light Source (ALS, beam line 8.2.1) at a temperature of 100 K. Prior to freezing, the corresponding crystals were picked with a CryoLoop (0.2~0.3 mm diameter, Hampton Research) and then soaked for 3min in cryoprotectant (25% glycerol in its reservoir solution). To prevent crystal damage by x-ray beam during data collection, crystals were frozen in liquid nitrogen before x-ray irradiation. Crystals were positioned and rotated based on a data collection strategy from HKL2000 software (HKL research Inc.).

Heavy atom soaking method: Since truncated junctin contains glutamic acids toward the C-terminus and serines and arginines are scattered throughout the sequence, lead and bromine were chosen as potential heavy atoms to bind to them. A small amount of NaBr (Fisher Scientific, New Jersey, USA) and tributyllead acetate (Alpha Inorganics Ventron, Massachusetts, USA) were dissolved in the crystallizing reservoir solution containing 25% glycerol and the final solution was diluted to make a 5% glycerol containing solution. Junctin crystals were soaked initially in 5% glycerol containing solution and transferred into 25% glycerol containing heavy atom solution for 10min. After transfer to non heavy atom containing cryo solutions, the crystals were frozen in liquid nitrogen for data collection.

Selenium methionine substituted junctin expression and purification: To generate mutated junctin at Leu56, Leu75, Ile138 and Leu 157 residues, a QuikChange XL Site-Directed Mutagenesis Kit (Stratagene, La Jolla, CA) was used and the resulting mutations were confirmed through DNA sequencing. For selenomethionyl-labelled protein, cells were transformed into *E.coli* B834 cells and an overnight culture was harvested. After

transformation, cells were initially grown in M9 medium containing 30 μg/ml kanamycin and supplemented with 2 mM $MgSO_4$, 2mM $FeSO_4.7H_2O$, 0.4% glucose, 1mg/ml of Nicinamide, Pyridoxine HCl, Thiamine, respectively, 0.1 mM $CaCl_2$, 4mg/ml of 19 amino acids and methione and finally, the culture was transferred into the large scale flask, and 10 mg/ml selenomethionine (^{Se}Met) was substituted for methione in this media. The culture was grown at 37 °C and induced at OD_{600} 0.8 with 0.5 mM IPTG at 30ºC for 10 hours. Harvested cells in wash buffer (50mM NaH_2PO_4, 300mM NaCl, 20mM imidazole pH8.0, 1mM DTT) were disrupted using a sonifier (VWR), followed by centrifugation at 20,000g for 40 minutes. The supernatant was applied into a pre-equilibriated Ni-NTA (Qiagen) column with a wash buffer and the column was washed with 15 column volumes of the wash buffer followed by protein elution. The elution buffer contained 50mM NaH_2PO_4, 300mM NaCl, 250mM imidazole with a final pH 8.0 and 1mM DTT. The methods need for further purification are the same as described in **Methods**.

Results and discussion

Canine cardiac junction was successfully overexpressed in *E.coli*, purified (Fig.1) and crystallized (Fig.2). However, there is no atomic model to estimate the initial phase of junctin diffraction data. Therefore, the phase problem to overcome for the determination of junctin structure from diffraction data is being approached by Multiple Isomorphous Replacement (MIR) and the Multiple wavelength Anomalous Dispersion (MAD).

In the case MIR, the application of the method is briefly explained as follows and the more detail method description is in **SUPPLEMENTS**. Two chosen heavy atom compounds to soak the native crystal, lead (Pb) and bromine (Br), turned out to be reactive with junctin molecules.

For MAD, Selenium Methione (^{Se}Met) substituted protein was prepared as described in **Methods**. Due to the absence of methione residues in the truncated junctin, the secondary structural elements were predicted from its primary sequence and leucines and isoluecine with a similar size to that of methione were selected and they were mutated to methiones for selenium methione substitutions.

Table. 1 Primers for methionine Substitution. Codons corresponding to Leu 56 ,75 and 157 and Ile 138 were mutated for Met substitutions. The positions of "atg" codons in the primers are in bold.

L56M

5' atg aag aag ttt tag gaa aa**a** **tg**g gag tct atg atg ctg atg gt
3' acc atc agc atc ata gac tcc cat ttt tcc taa aac ttc ttc at

L75M

5' atg tgg atg atg cca aag tt**a** **tg**c tag aag gac ctg gtg ggg ta
3' tac ccc acc agg tcc ttc tag cat aac ttt ggc atc atc cac at

I138M

5' aga aaa ttg ctg atg cag at**a** **tg**t cca gga aag aat ctc caa ag
3' ctt tgg aga ttc ttt cct gga cat atc tgc atc agc aat ttt ct

L157M

5' gag aga agg aga atg tgg gc**a** **tg**g aca aaa gtg cta aag cca ag
3' ctt ggc ttt agc act ttt gtc cat gcc cac att ctc ctt ctc tc

Table. 2 Data collection statistics. Values in parentheses indicate for the highest resolution shell.

Spacegroup	*I422*
Unit cell dimensions	121.37 121.37 136.64
	90 90 90
Resolution range	45.37-1.99 (2.07-1.99)
Total number of reflections	276742
Number of unique reflections	34777
Average redundancy	7.96 (5.85)
% completeness	99.4 (94.2)
Rmerge	0.125(0.620)
Reduced ChiSquared	1.01(1.17)
Output<I/SigI>	7.3 (2.6)

Figure legends

Fig. 1, Purified recombinant canine cardiac junctin. SDS PAGE (15%) was stained with Coomassie Blue staining solution. From *lane 1* to *lane 10*, control *E.coli* cell (ER2566) without IPTG, cell pellet after lysis, supernatant after lysis, flowthrough, wash, eluate 1,2,3,4,5, respectively.

Fig. 2, Crystals of canine cardiac junction and X-ray diffraction pattern of junctin crystals. Hexagonal shaped crystals were grown at 4ºC. After one month of growth, they were data collection quality.

Fig. 3, Predicted secondary structural elements of junctin from its primary sequence. The secondary structure for junctin was predicted through the software, SDSC biology workbench (Sandiego supercomputer center, http://workbench.sdsc.edu/). The secondary structural elements are in colored as described in the figure. The positions of mutated methiones are underlined. As shown in Fig. 3, there are 5 predicted α helices and 6 β sheet strands with loops or random coils in the remainder sequence.

Fig. 1

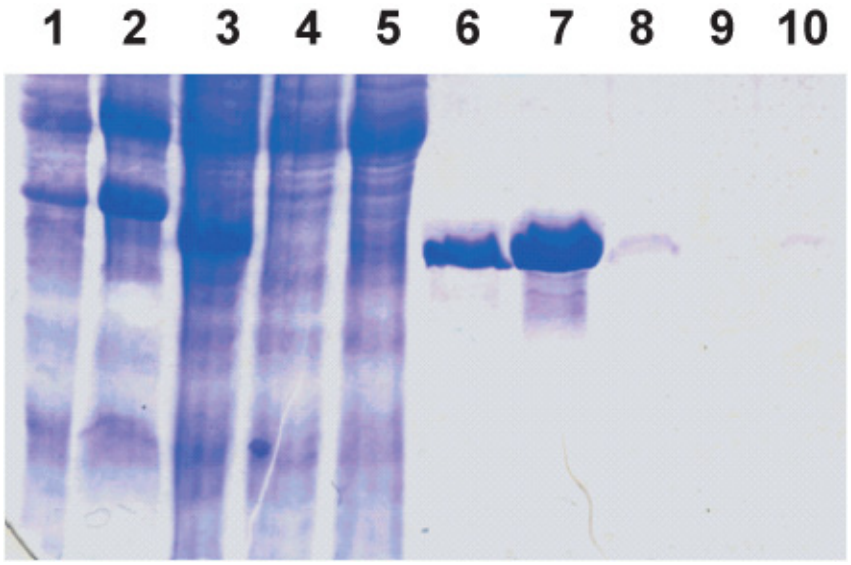

Fig. 2

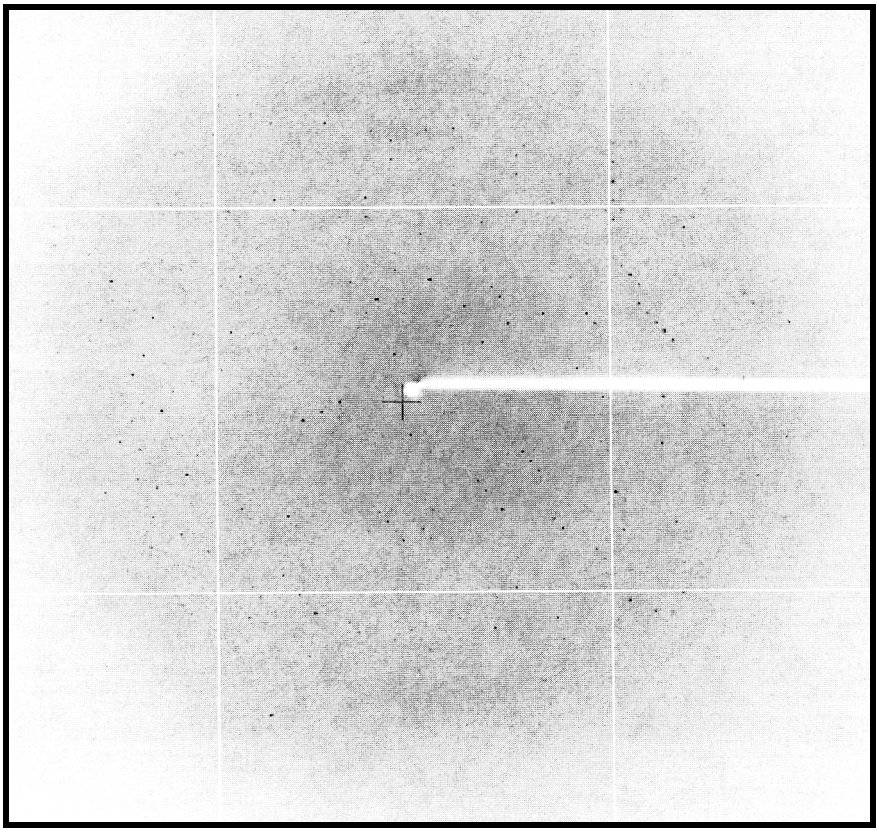

Fig. 3


N-FDLVDYEEVLGKLGVYDADGDGDFDVDDAKVLLEGPGGVAKRKTKAKVKE
LTKEELKKEKEKTESRKENKNEERRKGKKEKEDERKDKKIADADISRKESPK
GKKDREKENVGLDKSAKAKESRKKSTNVKDASSKTASRDKDDTKEGKTS
SKHTHSAKGNNQKRKN-C
56
75
138
157
LEGEND:
Alpha Helix = Red Beta Sheet = Blue Random Coil = Black

References

1. **L. Zhang, J. Kelley, G. Schmeisser, Y.M. Kobayashi, and L.R. Jones .** (1997) *J. Biol. Chem.*, 23389–23397.

2. **C. Franzini-Armstrong Protasi, and P. Tijskens.** (2005) *Ann. NY Acad. Sci.*,**1047**, 76–85.

3. **D. N. MacLennan, and P. Wong.** (1971) *Proc Natl Acad Sci* USA, **68**, 1231-1235.

4. **H**. **Park , I-Y. Park, E. Kim, B. Youn, K. Fields, A. Dunker, and C. Kang.** (2004) *J. Biol.Chem.*, **279**, 18026-18033.

5. **D. N. MacLennan, N. Abu-Abed, and C. Kang.** (2002) *J. Mol. Cell Cardiol.*, **34**, 897-918.

6. **D**.**Terentyev , I. Gyorke, P. Volpe, S. Williams, and S. Gyorke.** (2003) *Proc Natl Acad Sci USA,* **100**, 11759-11764.

7. **N. Beard, D. Laver, and A. Dulhunty.** (2004) *Prog. Biophys Mol. Biol.,* **85**, 33-69.

8. **R. D., Mitchell, H. K. B.,Simmerman, and L. R. Jones.** (1988) *J. Biol.Chem.*, **263**, 1376-1381.

9. **L.R. Jones, L. Zhang, K. Sanborn, A.O. Jorgensen, and J. Kelley.** (1995) *J. Biol. Chem.*, **270**, 30787–30796.

SUPPLEMENTS

Multiple wavelength Anamalous Dispersion method (MAD):

The x-ray diffraction data for canine cardiac junctin has been collected up to 2.6 Å resolution. In order to solve the phase problem of junction diffraction data, multiple wavelength anomalous dispersion method (MAD) and multiple isomorphous replacement method (MIR) are going to be applied due to its lack of sequence similarity with other known structures at present.

The primary difficulty in macromolecular X-ray crystallography is the "Phase problem". This is a problem of determining the phase angle to be associated with each structure factor, so that an electron density map may be calculated from a Fourier series with structure factors as coefficients. Generally, there are several methods available for overcoming this fundamental problem: They are Molecule Replacement, Multiple Isomorphous Replacement (MIR), Multiple Wavelength Anomalous Dispersion (MAD), Single Isomorphous Replacement (SIR) and Direct Methods, but the most practical ones in macromolecular crystallography are Molecular Replacement, Multiple Isomorphous Replacement (MIR) and Multiple wavelength Anomalous Dispersion (MAD). In Junctin structure determination, we applied the Multiple Isomorphous Replacement (MIR) method.

Concepts for anomalous scattering: Generally, electrons in an atom are regarded as free electrons, which have a phase difference of 180º with respect to the incident beam. When the x-ray wavelength approaches an absorption edge, scattered x-ray maximizes an imaginary component to its phase (f'' scattering coefficient becomes non-zero) because of

retardation compared to a normally scattered x-ray. The atomic scattering factor f of anomalous scattering can be written as

$$f_{anom} = f + f^{'} + if^{''} \qquad \text{Eq.1}$$

where $f^{'}$ and f'' are real and imaginary contributions of anomalous signal, respectively. Anomalous scattering does not follow *Friedel*'s Law (1) which states, "*members of a Friedel pair have equal amplitude and opposite phase (Fhkl = F$\overline{hkl}$)*". The real scattering component $f^{'}$ is related to f'' via the *Kramers-Kronig* relationship (2; 3). This anomalous behavior can be used for the structure determination.

Changes in the protein structure factor are induced by tuning the X-ray wavelength to different points in the absorption spectrum of the incorporated heavy atom, thus changing the values of the anomalous scattering factors $f^{'}$ and f'', which in turn affect the structure factor. In MAD, this may be achieved by measuring diffraction data at least two X-ray energies. Usually diffraction data sets are collected at three different X-ray energies; the edge, where $f^{'}$ is minimum; the peak, where f'' is maximum and the *Friedel* pair has the largest difference; the remote, where $f^{'}$ and f'' and are small (3; 4).

Algebraic process: Each anomalously scattering atom has an atomic scattering factor of $f = f_0 + f' + if''$ (Eq 1)(1). In the complex vector diagram (Fig.1), F_B is the contribution to the structure factor by the nonanomalously scattering atoms, F_A is the nonanomalous contribution of the anomalously scattering atoms, and the complete nonanomalous part is $F_{BA} = F_B + F_A$.

Fig.1

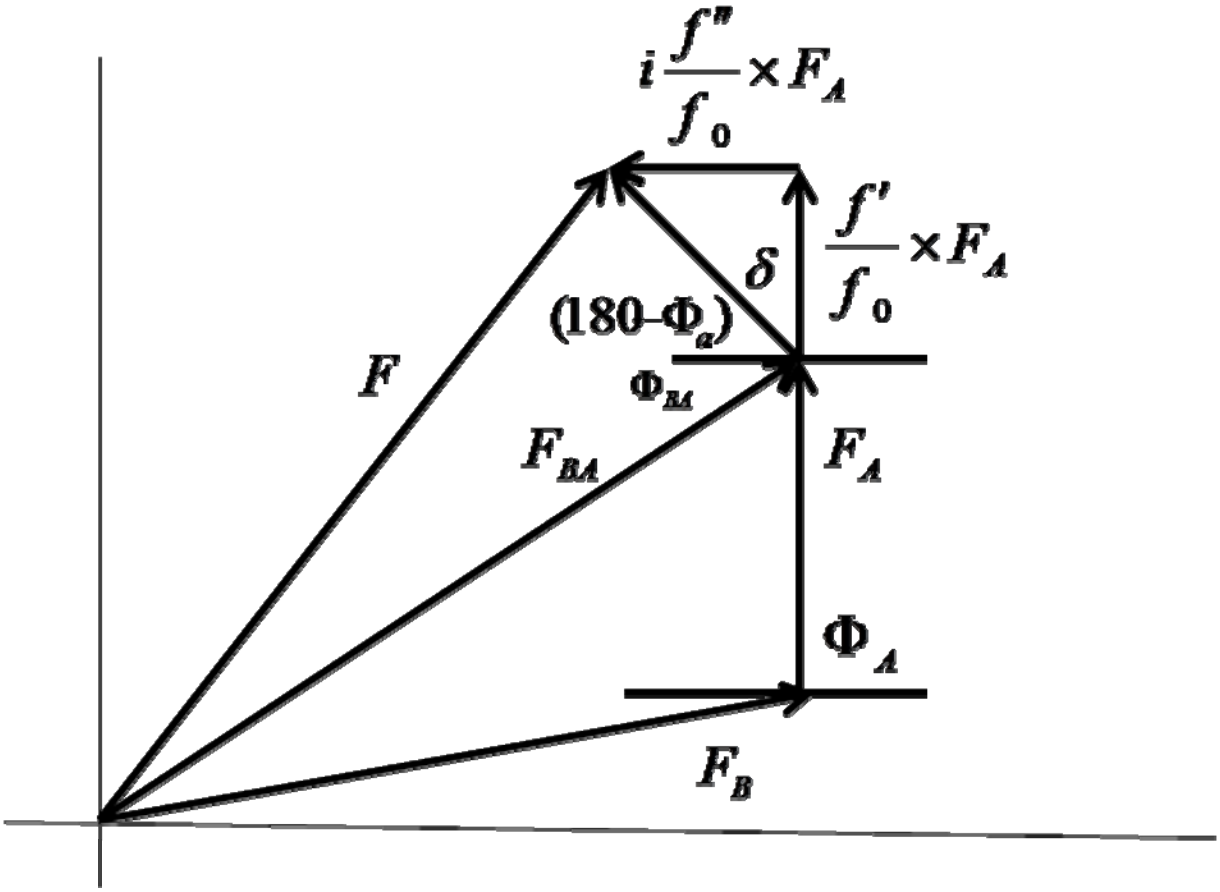

The anomalous scattering contribution, a , is

$$a = \frac{f'}{f_0}\times F_A + i\frac{f''}{f_0}\times F_A$$

Φ_{BA} is the phase angle of F_{BA} , Φ_A of F_A , and Φ_a of vector F_A , and Φ_a of vector a.

$$\Delta\Phi = \Phi_{BA} + (180 - \Phi_a) = 180° + (\Phi_{BA} - \Phi_a).$$

Amplitude of the structure factor F is

$$|F|^2 = |F_{BA}|^2 + |a|^2 - 2|F_{BA}| \times |a| \times \cos \Delta\Phi \qquad \text{Eq.3}$$

with

$$|a|^2 = \frac{(f')^2 + (f'')^2}{f_0^2} \times |F_A|^2,$$

$$|F|^2 = |F_{BA}|^2 + \frac{(f')^2 + (f'')^2}{f_0^2} \times |F_A|^2 + 2\frac{f'}{f_0} \cos\delta |F_{BA}| \times |F_A| \cos(\Phi_{BA} - \Phi_a)$$
$$+ 2\frac{f''}{f_0} \sin\delta |F_{BA}| \times |F_A| \cos(\Phi_{BA} - \Phi_a)$$

and this can be rewritten as

$$|F|^2 = |F_{BA}|^2 + p|F_A|^2 + |F_{BA}| + |F_A| \times [qcon(\Phi_{BA} - \Phi_A) + r\sin(\Phi_{BA} - \Phi_A)\ ]$$

with $p = \frac{(f')2 + (f'')2}{f^2{}_0}, q = 2\frac{f'}{f_0} \quad r = 2\frac{f''}{f_0}$

p, q and r are functions of wavelength and can be derived from the atomic absorption coefficient. $|F|^2$ can be determined experimentally. Unknown quantities $|F_{BA}|, |F_A|$ and $(\Phi_{BA} - \Phi_A)$ are independent of wavelength and equal for *Friedel* pairs, except for the sign of $(\Phi_{BA} - \Phi_A)$. Therefore, a minimum of two different wavelengths is sufficient to find $|F_{BA}|, |F_A|$ and $(\Phi_{BA} - \Phi_A)$ for each reflection. Φ_{BA} can obtained by calculating Φ_A, which can be derived from a Patterson map with coefficients $|F_A|^2$ or by direct methods.

Because no anomalous scattering is taken into account for the calculation of the structure, the real phase or its enantiomorph is obtained for F_A . The solution for this is to calculate Φ_A for both structures. This gives two solutions for Φ_{BA} and best electron density map will be the final solution (2).

References

1. Hauptman H. Acta Crystallogphyca Section D. 49, 3-8, (1993)

2. Drenth, J. Principles of protein X-ray crystallography, 2nd Ed., Springer-Verlag, Inc (1999).

3. McRee, D. Practical protein crystallography, 2nd Ed., Academic press (1999).

4. Phodes, G. Crystallography made crytal clear, 2nd Ed., Acedemic press (1999).

OVERALL PROCESS OF MULTIWAVELENGTH ANOMALOUS DISPERSION

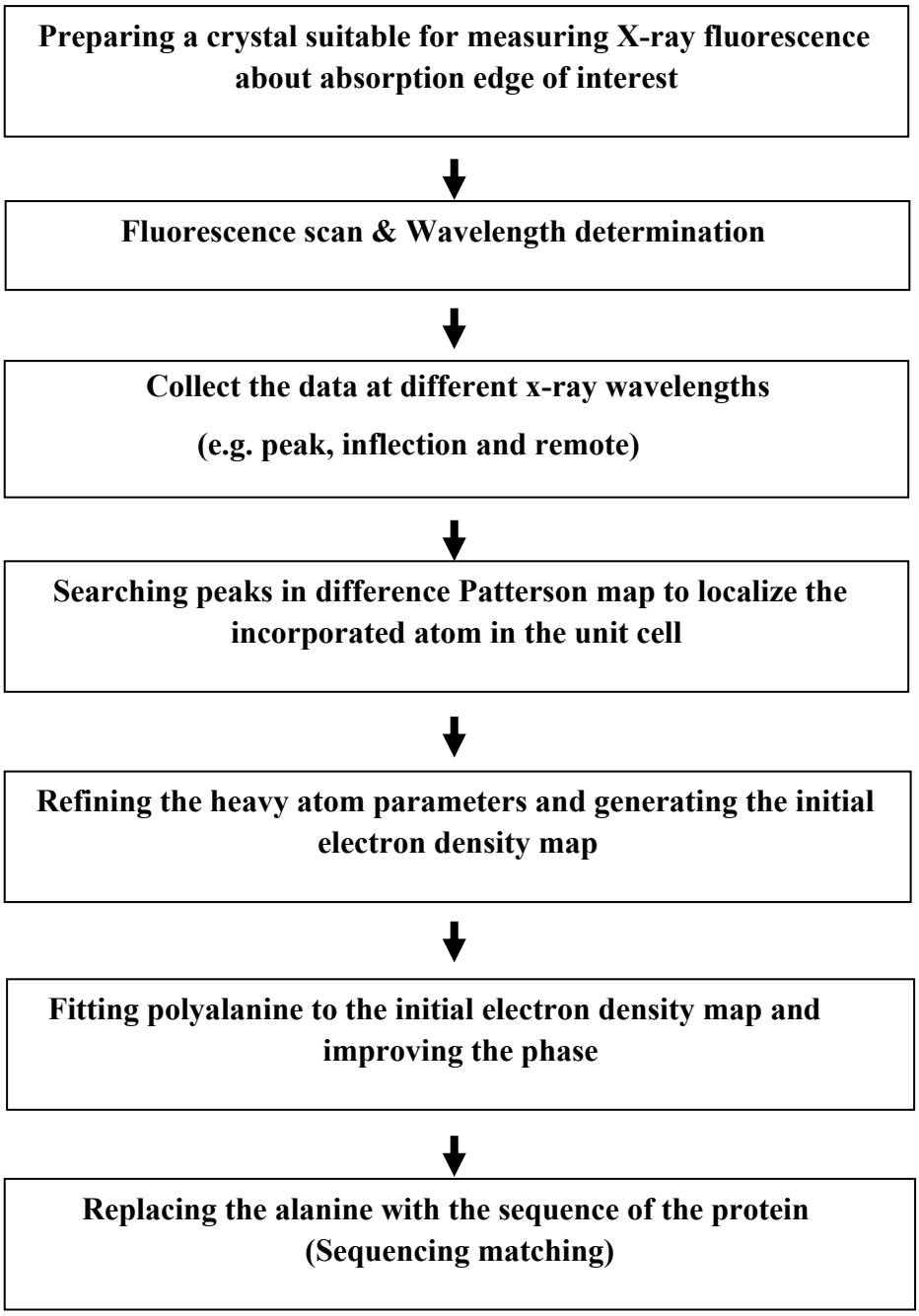

Multiple Isomorphous Replacement Method (MIR)

Concepts

Isomorphous replacement method, developed by Green, Ingram and Perutz, is still one of the most popular phasing methods and it is, except MAD, the only method available for solving the protein structures with very limited structure information.

Application of the isomorphous replacement method requires the X-ray diffraction data of the native protein crystal as well as that of the heavy atom derivative crystal. The single isomorphous replacement method (SIR) and multiple isomorphous replacement (MIR) are based on the introduction of one or more heavy atoms as new scatters of high atomic number without disturbing the crystal packing or molecular structure. For perfect isomorphism, the conformation of the protein, the position and orientation of its molecules as well as the unit cell parameters in the native and in the derivative crystals must be exactly same. Under this restricted conditions, the intensity differences between the native and the other patterns are then exclusively due to the attached heavy atom.

F_P is the structure factor of protein, $|F_P|$ with its magnitude and Φ_P with its phase. F_{PH} is contribution from the heavy atom plus protein. If perfect isomorphism is assumed, structure factor of the heavy atom isomorphous derivatives are simply defined as Eq.1

$$F_{PH} = F_P + F_H \qquad \text{Eq.1}$$

where F_H is the structure factor contribution from the heavy atom only. The final goal is to derive a value of $\Phi H'$, but only $|F_P|$ and $|F_{PH}|$ can be measured. $|F_H|$ can not be measured but can be calculated by means of *difference-Patterson*-techniques (3). Once the position of the heavy atom is more or less accurately determined, the calculated value of Φ_H can be used to estimate angle of structure factor of the native protein

$$\Phi_P = \Phi_H + \cos^{-1} [(|F_{PH}|^2 - |F_P|^2 - |F_H|^2) / 2|F_P||F_H|] \qquad \text{Eq.2}$$

Since this equation contain and inverse cosine term, two solutions can exist for Φ_P. This ambiguity is illustrated in Fig.1. Actually, the MIR was the first method to solve the phase ambiguity.

Fig.1

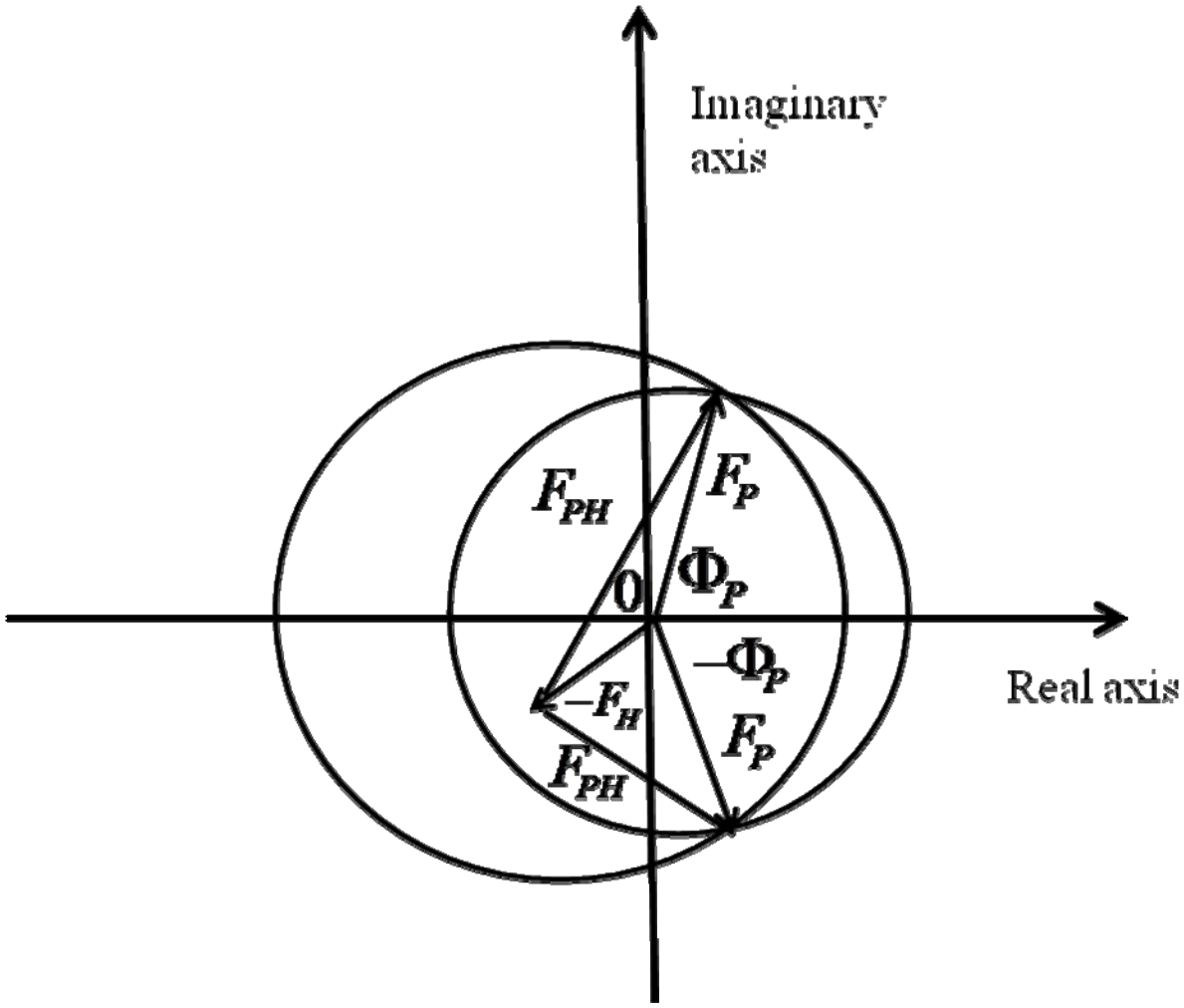

It is based on second heavy atom bound to the protein molecule in a position different from the first one. Therefore, both heavy atom positions must be derived (2;4;5;6). The graphical construction in Fig.2 is equivalent to solving the pair of simultaneous equations occurring in Eq.3.

Fig.2

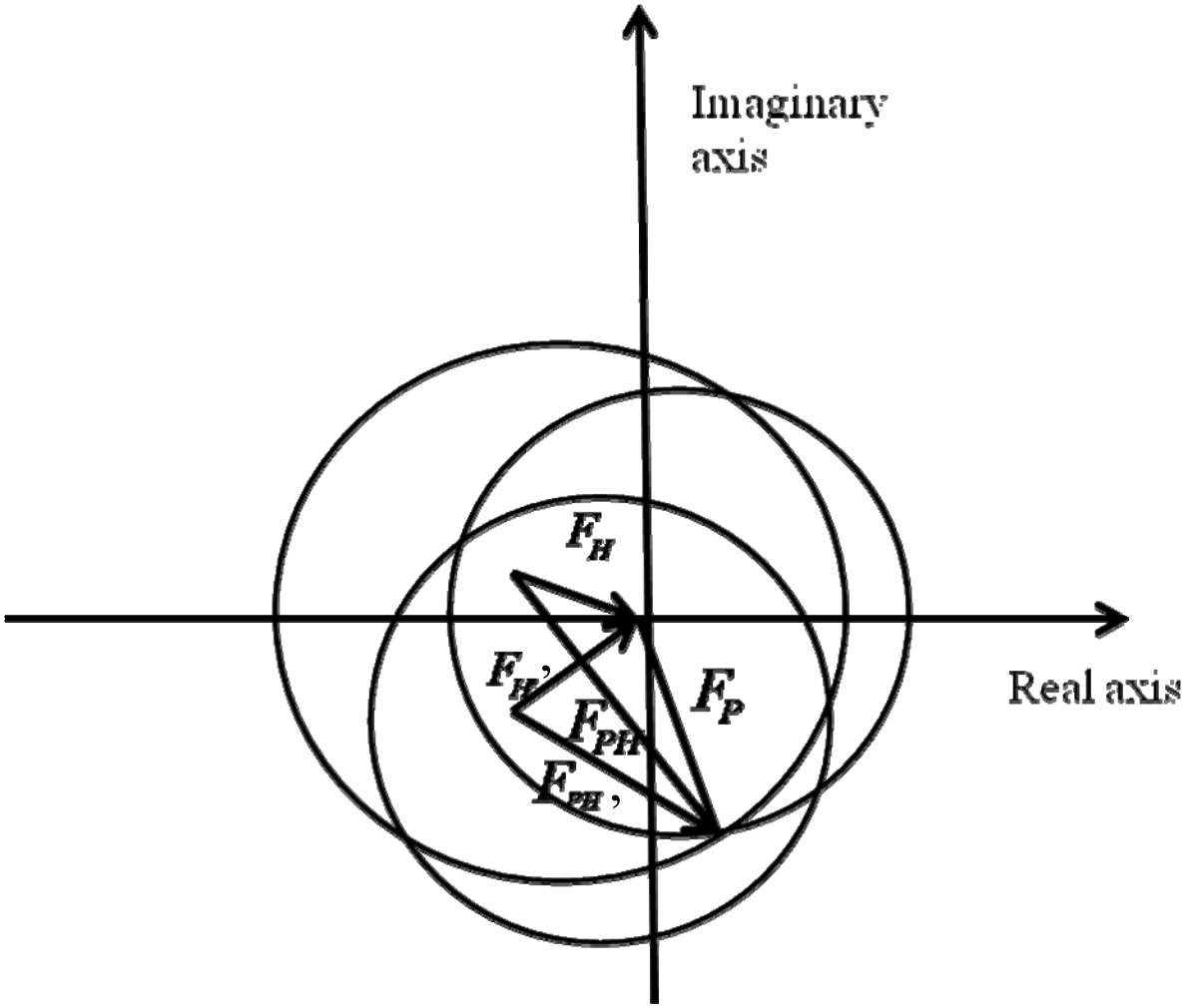

$$\Phi_P = \Phi H + \cos^{-1}[(|F_{PH}|^2 - |F_P|^2 - |F_H|^2)/2|FP||FH|]$$
$$\Phi_P = \Phi_{H'} + \cos^{-1}[(|F_{PH}|^2 - |F_P|^2 - |F_H|^2)/2|F^P||F_{H'}|]$$

Theoretically, two different heavy atom derivatives yield an unambiguous value for the phase angle of the native protein, but even small experimental errors in the amplitude will

lead to rather uncertain phases. Therefore, in practice, we need more than two derivative data and a sophisticated weighting algorithm to sort this ambiguity.

The phasing power of Heavy atom

The phasing power and figure of merit are the most popular way to judge the quality of phasing by MIR. Following are the mathematical basis for these concepts. This part is based on Appendix 2 in the "*Principle of Protein X-ray Crystallography*", by Jan Drenth.

Isomorphous phasing power:

$$\sqrt{\frac{\sum_{hkl}\left|F_H(calc)\right|^2}{\sum_{hkl}\left|E\right|^2}}$$

with $\sum_{hkl}\left|E\right|^2 = \sum_{hkl}[\left|F_{PH}(obs)\right| - \left|F_{PH}(calc)\right|]^2$

Alternative expression is: $$\frac{\sum_{hkl}\left|F_H(calc)\right|}{\sum_{hkl}\left|E\right|}$$

The figure of merit for a given reflection (*h k l*) is defined as

$$m = \frac{\left|F(hkl)best\right|}{\left|F(hkl)\right|}$$

Where $$F(hkl)best = \frac{\sum_{\alpha} P(\alpha)Fhkl(\alpha)}{\sum_{\alpha} P(\alpha)}$$

It can be shown that the figure of merit is the weighted mean fo the cosine of the deviation of the phase angle from α_{best} : $m = \cos[\alpha - \alpha(best)]$.

References

1. Green, D.W.,Inggram, V.M. and Perutz M.F. (1954) Proc. Roy. Soc. 225, 287-307
2. Drenth, J. (1999) Principle of protein X-ray crystallography, 2nd., Springer Verlag, Inc.
3. Reed RJ.(2003) Acta Crystallogr D. 59,1881-1890
4. MacRee, D. (1999) Practical protein cdrystallography, 2nd., Academic press
5. Karle J.(1989) Actaa Crystallogr A. 45,765-781
6. Rhodes, G. (2000) Crystallography made crystal clear, 2nd., Academic press

OVERALL PROCESS OF MULTIPLE ISOMORPHOUS REPLACEMENT